学位申請論文

加藤立久

学 位 審 査 報 告

氏　　名	加　藤　立　久
学位の種類	理　学　博　士
学位記番号	論　理　博　第　　号
学位授与の日付	昭和　　年　　月　　日
学位授与の要件	学位規則　第5条　第2項該当

（学位論文題目）

State selected charge transfer reactions in the $BC^+ + Ar \rightleftarrows BC + Ar^+$ systems : Comparison among $BC = H_2$, O_2, and NO

$BC^+ + Ar \rightleftarrows BC + Ar^+$ 系における状態を選別した電荷移動反応の研究 : BCとしてH_2, O_2, NOを用いた時の比較

論文調査委員	主　査　志　田　忠　正 波多野　博　行，　廣　田　　襄

理　学　研　究　科

氏　名	加　藤　立　久

（論文内容の要旨）

原子，分子の二分子的電荷移動反応の機構については従来，現象論的に「直接機構」と「複合体機構」があるとされてきたが詳細な分子論的解析はほとんどなされていなかった。本研究ではH_2，O_2，NO分子にArイオンを衝突させたときの電荷移動反応とその逆反応をとりあげ，反応機構を解明する目的で二原子分子イオンについてはその振動状態，またArイオンについては全電子角運動量を指定した上で両方向反応の相対的反応断面積を測定した。実験結果は反応ポテンシャル面によって解析し，その結果，「直接機構」，「複合体構」の内容についての理解を得ることができた。

先づ　$H_2^+ + Ar \rightleftarrows Ar^+ + H_2$ は「直接機構」で起ることが知られている系であるが，この系については始状態と終状態の（$Ar \cdots\cdots H_2$）間距離が無限大でのエネルギー差（△E）が小さく，また，フランク－コンドン因子（FC因子）が大きい内部状態（H_2^+ は $\tilde{X}\ ^2\Sigma_g^+$，$v=2$，Ar^+ は $^2P_{\frac{1}{2}}$）の反応において断面積が共鳴的に大きくなることを実験的に見出した。この結果はRapp－Francisの取扱いを拡張したモデルによる計算でもよく再現されることが判った。反応が（$Ar \cdots\cdots H_2$）間距離無限大での△EとFC因子で支配される理由は，次の様に考えられる。$(H_2 + Ar)^+$ 系の始状態と終状態の2枚のポテンシャルは，（$Ar \cdots\cdots H_2$）間距離（分子間距離）無限大でH－H核間距離方向（分子振動方向）にもともとcrossingをもち，大きな分子間距離で非交叉する。そのため，電荷移動はこの分子振動方向のavoided crossingを経由して大きな分子間距離で始まり，分子間距離方向のavoided crossingと無関係に直接，電子が長距離移動するためとして理解された。

次に $O_2^+ + Ar \rightleftarrows Ar^+ + O_2$ については O_2^+（$\tilde{a}\ ^4\Pi_u$，v）＋Arから出発する反応は△E，FC因子で支配される「直接機構」であるが，逆の Ar^+（^2P_J）＋O_2から出発する反応についてはJ依存性がないことが判った。この結果を説明するためにAr^+（^2P_J）＋O_2（$\tilde{X}\ ^3\Sigma_g^-$）から生成する直線型複

合体には2つの四重項の他に2つの二重項状態があり得ることに着目し，正方向の O_2^+（$\tilde{a}\ ^4\Pi_u$, v）＋Ar→は四重項ポテンシャル面上で進行するものの，逆方向の Ar^+（^2P_J）＋O_2（$\tilde{X}\ ^3\Sigma_g^-$）→については二重項ポテンシャル面上で進むものと推論した。この逆反応は先づ Ar^+（^2P_J）＋O_2（$\tilde{X}\ ^3\Sigma_g^-$）とエネルギー的に近接した別の二重項状態，O_2^+（$\tilde{A}\ ^2\Pi_u$）＋Ar，が相互作用して反応系を安定化させ，その結果として終状態，O_2^+（$\tilde{X}\ ^2\Pi_g$）＋Arとavoided crossingを起こし，この交叉点で非断熱的に電荷移動するものと考えた。このような遷移は（O_2……A_r）間距離が小さくなったときに起るため，（H_2＋Ar）$^+$ 系のように△Eと FC因子とに関係づけて議論することは無意味の筈で，事実，上の逆反応は△E，FC因子と無関係で，従来からの「複合体機構」に対応するものと見做せる。

最後に NO^+（$\tilde{a}\ ^3\Sigma^+$, v）＋Ar⇄Ar^+＋NO の正反応については実験およびモデル計算ともに大略は△E，FC因子で支配される「直接機構」を示唆するが詳細に検討すると正反応の一部および逆反応は（NO …… Ar ）が垂直および直線状に配置した複合体を経由する機構も存在することを示している。この点を明らかにする目的で藤永の MIDI-4 基底関数（GTO）を用いたab initio MO計算を行い，NO^+（$\tilde{a}$）＋Ar に漸近する垂直型複体と，Π状態の平行型複合体が形成されることを確めることができた。結局，上のように2種類の複合体が生成することが（NO＋Ar）$^+$ 系の反応の特長を説明することが判った。

氏　名	加　藤　立　久

（論文審査の結果の要旨）

化学反応は一般に非常に多くの量子状態に熱的に分布した分子の間で統計的過程として進むのでその分子論的解析は容易でない。本論文は最近の化学反応研究の最先端である量子状態を指定した原子，分子間の反応を扱い，その機構を分子論的に解析したものである。

具体的にはH_2，O_2，NO分子にArイオンを衝突させたときに起る電荷移動反応とその逆反応をとり上げ，「しきい電子，二次イオン同時計数法」（通称ＴＥＳＩＣＯ法）を用いて二原子分子イオンについてはその振動量子数を，またＡｒイオンについては全電子角運動量子数を指定した上で上記の正逆反応の相対的断面積を測定し，その結果を衝突理論および分子軌道理論によって解析した。ＴＥＳＩＣＯ法は反応系の原子，分子を光イオン化するに足りる最小のエネルギーの光子で照射し，発生する親イオンを電場内で加速して一定の運動エネルギーを与えた上で反応相手の原子，分子と衝突させ，電荷移動反応で生成する二次イオンの内，親イオンと共に生じた運動エネルギーがゼロのしきい電子と同期した二次イオンのみを計数することで状態を選別した電荷移動反応の断面積を求める方法である。この方法は申請者らが考案，製作し現在，世界的に見ても比肩するものが見当らないものである。申請者はこの方法を用いて精力的に実験を行い，また理論的解析の方法を工夫し従来，現象論的に「直接機構」と「複合体機構」に分類されていた電荷移動反応の内容に分子論的解釈を与えた。具体的な知見はつぎの通りである。

1）$(Ar+H_2)^+$ 系での電荷移動は正逆両反応ともArとH_2の距離が比較的大きい領域で電子の長距離移動によって完了する。このためArとH_2の距離が大きいときのエネルギー差と，フランク－コンドン因子とで断面積を議論することが可能で，エネルギー差がゼロに近いとき共鳴的に断面積が大きくなる。この系は従来の「直接機構」の典型例となっている。

2）$(Ar+O_2)^+$ 系では，四重項状態のO_2^+（$\tilde{a}\ ^4\Pi_u$）から出発する反応

は（$Ar + H_2$）$^+$系と同様に「直接機構」で進むが，Arイオン（^2P_J）から出発する反応は二重項ポテンシャル面上で進み，始状態，終状態とは別の第三の二重項状態の影響を受けて（O_2 ……Ar）間距離の小さなavoided crossing pointで非断熱的に電荷移動する。この反応は従来の「複合体機構」の一つの例となっている。

3）（$Ar + NO$）$^+$系では，「直接機構」で反応が進むと並行して「複合体機構」による反応も起り，且つ複合体としてはＮＯ分子に接近するＡｒがＮＯの分子軸に平行か或は垂直かによって異る複合体を経由した反応を起こす。

以上，本論文は状態選別化学反応を高度な実験方法により研究し，大胆なモデルで解析して反応の本質を把握することに成功したもので理学博士の学位を授与する価値のあるものと認める。

なお，主論文および参考論文に報告されている研究業績を中心としてこれに関連した研究分野について試問した結果，合格と認めた。

学位申請論文内容説明要旨

氏　　名　　加　藤　立　久

出身学校　　京都大学大学院理学研究科
（化学専攻）　　修士課程
昭和54年3月　　修　了

論文題目　　$BC^+ + Ar \rightleftarrows BC + Ar^+$ 系における状態を選別した電荷移動反応の研究：BCとしてH_2, O_2, NO を用いた時の比較

主論文　　State selected charge transfer reactions in the $BC^+ + Ar \rightleftarrows BC + Ar^+$ systems : Comparison among BC = H_2, O_2, and NO

The Journal of Chemical Physics, Vol. 80, No. 12 (1984).
掲載予定

参考論文

1. Photoinduced isomerization of ion radicals. The conversion from 1,3-cyclohexadiene to 1,3,5-hexatriene cation radicals.
The Journal of Physical Chemistry, Vol. 81, 1095-1103(1977).
(志田忠正、野坂芳雄と共著)

2. Electronic absorption spectra of some cation radicals as compared with ultraviolet photoelectron spectra
The Journal of Physical Chemistry, Vol. 82, 695-698(1978).
(志田忠正、野坂芳雄と共著)

3. Electronic structures of ion radicals of N-heteroaromatic hydrocarbons as studied by ESR and optical spectroscopy
The Journal of the American Chemical Society, Vol. 101, 6869-6876(1979).
(志田忠正と共著)

4. ESR and optical studies on the cation-radical of pyridine in a γ-irradiated rigid matrix at low temperatures
Chemical Physics Letters, Vol. 68, 106-110(1979).
(志田忠正と共著)

5. ESR studies on cation-radicals of simple olefins and dienes produced in γ-irradiated frozen solutions of trichlorofluoromethane

   The Journal of Chemical Physics, Vol. 73, 5963-5970(1980).

   (志田忠正、江川嘉一、久保寺英夫と共著)

6. Direct determination of individual reaction cross sections for the two spin-orbit states $Ar^+(^2P_{3/2}, {}^2P_{1/2})$

   The Journal of Chemical Physics, Vol. 73, 586-588(1980).

   (田中健一郎、Jean Durup 、小谷野猪之助と共著)

7. State selected ion-molecule reactions by a TESICO technique.

   II. Separation of the reactant spin-orbit states in the reaction

   $Ar^+(^2P_{3/2},{}^2P_{1/2}) + H_2(D_2) \rightarrow ArH^+(ArD^+) + H(D)$

   The Journal of Chemical Physics, Vol. 74, 5561-5571(1981).

   (田中健一郎、Jean Durup 、小谷野猪之助と共著)

8. State selected ion-molecule reactions by a TESICO technique.

   III. $H_2^+(v) + Ar \rightarrow ArH^+ + H$, $Ar^+ + H_2$: Observation of enhanced charge-transfer cross sections at near resonance

The Journal of Chemical Physics, Vol. 75, 4941-4945(1981).
(田中健一郎、小谷野猪之助と共著)

9. State selected ion-molecule reactions by a TESICO technique.
IV. Relative importance of the two spin-orbit states of Ar^+ in the charge transfer reactions with N_2 and CO
The Journal of Chemical Physics, Vol. 77, 337-341(1982).
(田中健一郎、小谷野猪之助と共著)

10. State selected ion-molecule reactions by a TESICO technique.
V. $N_2^+(v) + Ar \rightarrow N_2 + Ar^+$
The Journal of Chemical Physics, Vol. 77, 834-838(1982).
(田中健一郎、小谷野猪之助と共著)

11. State selected ion-molecule reactions by a TESICO technique.
VI. Vibronic-state dependence of the cross sections in the reactions
$O_2^+(X^2\Pi_g, v; a^4\Pi_u, v) + H_2 \rightarrow O_2H^+ + H,\ H_2^+ + O_2$
The Journal of Chemical Physics, Vol. 77, 4441-4446(1982).
(田中健一郎、Paul-Marie Guyon 、小谷野猪之助と共著)

12. State selected ion-molecule reactions by a TESICO technique.
VII. Isotope effect in the reactions $O_2^+(X^2\Pi_g, a^4\Pi_u) + HD \rightarrow O_2H^+(O_2D^+) + D(H)$

The Journal of Chemical Physics, Vol. 79, 4302-4305(1983).
(田中健一郎、Paul-Marie Guyon 、小谷野猪之助と共著)

13. State selected ion-molecule reactions by a TESICO technique.
VIII. Vibronic state dependence of the cross sections in the reaction $NO^+(a^3\Sigma^+, v; b^3\Pi, v) + Ar \rightarrow NO + Ar^+$

The Journal of Chemical Physics, Vol. 79, 5969-5974(1983).
(田中健一郎、小谷野猪之助と共著)

14. Analysis of the autoionization structure of N_2 using Ar charge exchange detection

Chemical Physics Letters, Vol. 97, 562-565(1983).
(田中健一郎、小谷野猪之助と共著)

15. New vibrational assignments for the autoionization bands of O_2 based on isotope shifts

The Journal of Chemical Physics, Vol. 81, No. 2(1984). 掲載予定

(西谷英輔、田中郁三、田中健一郎、小谷野猪之助と共著)

主　論　文　要　旨

電荷移動反応$A^+ + B \rightarrow A + B^+$は、二つのポテンシャル間での非断熱遷移によってひきおこされる。低エネルギー衝突での非対称電荷移動反応は、直接機構（direct mechanism）と複合体機構（intimate mechanism）に大別されているが、それぞれの機構をポテンシャル間の非断熱遷移と関連付けて本質的に説明した研究は少ない。一方、分子を含んだ系の電荷移動反応を、反応系と生成系の状態間のエネルギー準位差（ΔE）と Franck-Condon 因子（FC因子）の2つの物理量で説明する研究は多くあるが、反応物同志が無限に離れた始点と終点の間を性格付けるこれらの物理量が、低エネルギー衝突によるポテンシャル間の非断熱遷移を説明し得ることは不思議である。

今回、小谷野、田中らが発展させたしきい電子2次イオン同時計測法（Threshold Electron-Secondary Ion Coincidence : TESICO）を用いて、2原子分子 BC と Ar との間の電荷移動反応（$BC^+ + Ar \rightleftarrows Ar^+ + BC$）を調べた。TESICO 法は、反応イオンの量子状態を選別したイオン-分子反応断面積の直接測定を目的としており、単一の量子状態（BC^+ の振動（振電）状態、Ar^+ のスピン-軌道状態）からの電荷移動確率が得られ、ポテンシャル間の非断熱遷移の機構を知る上で有力な情報を与える。2原子分子 BC として、H_2、O_2、NO を用い、電荷移動反応断面積の選別状態依存性を比較した。その結果、$(BC + Ar)^+$ 系の低エネルギー衝突による電荷移動反応の二つの直接機構と複合体機構の本質的説明ができた。

1．モデル計算

二原子分子イオンBC^+の振動（振電）状態を選別したArへの電荷移動反応断面積、また逆にAr^+イオンのスピン－軌道状態を選別した二原子分子BCへの反応断面積、それぞれの選別状態依存性を反応系と生成系の間のエネルギー準位差（ΔE）、FC因子と比較するため、次の様なモデル計算を行なった。電荷移動後の生成系の終状態のそれぞれと選別した反応系の始状態とは、対をなす二準位として独立に扱えると仮定する。その二準位間$BC^+(v) + Ar \rightarrow BC(v') + Ar^+(^2P_J)$ または、$Ar^+(^2P_J) + BC(v=0) \rightarrow Ar + BC^+(v')$ の電荷移動反応断面積をRapp やFrancisの提出した二準位モデルの式に基づいてΔEの関数として扱う。対応する始、終状態間のFC因子を重みとして掛け合わせながら実験に用いた衝突エネルギーで到達可能な終状態にわたってたし合わせ、注目する選別状態からの電荷移動反応断面積とした。反応物の無限遠におけるこれら二つの物理量は、遠距離衝突で電荷移動のおこる直接機構を支配すると考えられる。

2．$(H_2 + Ar)^+$ 系

$H_2^+(X^2\Sigma_g^+)$の振動状態v＝0－4を選別したArへの電荷移動反応断面積の実験値とモデル計算値を二つの衝突エネルギーについて図1に示す。両衝突エネルギーとも、v＝2状態からの電荷移動反応断面積が顕著に増加している。この急激な増加はモデル計算からも得られ、反応系$H_2^+(X^2\Sigma_g^+, v=2) + Ar$ と生成系$Ar^+(^2P_{1/2}) + H_2(v=0)$の状態間

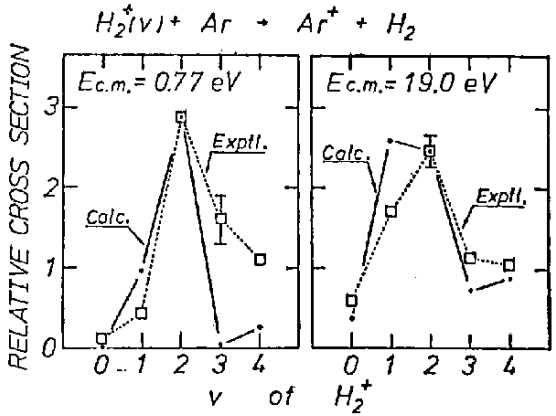

図　1

のエネルギー準位の近共鳴効果によると説明できる。また逆に、Ar^+ (^2P_J) のスピン－軌道状態 J ＝ 1／2 と 3／2 を選別した H_2 への電荷移動反応断面積の測定結果 [J ＝ 1／2 と 3／2 からの断面積の比 (σ(1／2 ／ σ(3／2)) の値] にも、同じ近共鳴効果による断面積の増加がみられる。（図2） $(H_2 + Ar)^+$ 系は、その電荷移動反応機構が ΔE と FC因子に支配される直接機構の典型例である。

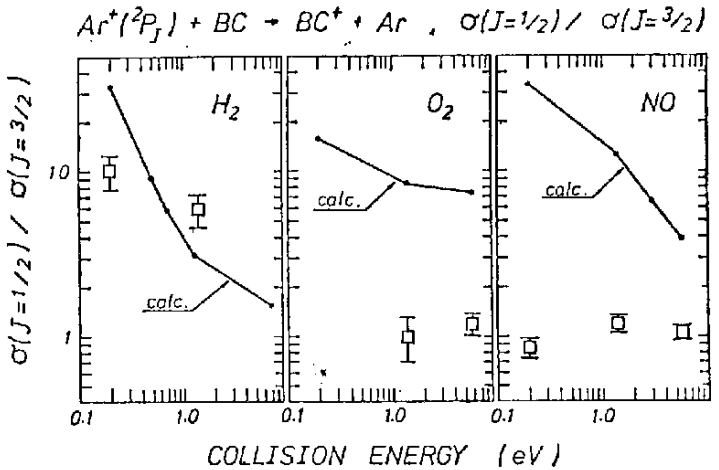

図 2

3．$(O_2 + Ar)^+$ 系

図3 に O_2^+ ($X^2\Pi_g$) の v ＝19、20、O_2^+ ($a^4\Pi_u$) の v ＝0 －7 状態を選別した反応断面積を示す。特に O_2^+ ($a^4\Pi_u$) での断面積の振動（振電）状態依存性は、H_2^+ からの場合と同様にモデル計算とほぼ一致しており、直接機構による電荷移動が起こっていることが解かる。ところが、逆に Ar^+ (^2P_J) から O_2 への電荷移動反応断面積のスピン－軌道状態依存性 [比 σ(1／2) ／ σ(3／2)] は、Ar^+ と H_2 の場合と異なりモデル計算の予想に反し、ほとんど選別状態に対して不変である。O_2^+ から Ar への電荷移動反応は直接機構によるが、Ar^+ から O_2 へのそれは直接機構によっていないという実験事実は、$(O_2 + Ar)^+$ 系のポテンシャル上でスピン状態が異なる（二重項、四重項）複数の電荷移動反応経路が存在することと関連している。また、Ar^+ から O_2 への電荷移動反応経路は、複合体機構による電荷移動に対応する。

4．$(NO + Ar)^+$ 系

$NO^+(a^3\Sigma^+) + Ar$ 状態と $Ar^+ + NO$ 状態は、NO^+ から Ar へまた Ar^+ から NO への電荷移動反応の始状態、終状態の関係にあり $(Ar + H_2)^+$ 系のエネルギー準位関係と類似しているため、両方向の電荷移動反応とも直接機構によると予想される。しかし、測定結果は図4に示す通り近共鳴による反応断面積の増加が、$NO^+(a^3\Sigma^+)$ の $v = 2$ にみられるものの、直接機構だけでは説明できない。事実、Ar^+ から NO への電荷移動反応断面積のスピン－軌道準位依存性はモデル計算結果に反する。この結果は $(O_2 + Ar)^+$ 系の場合と同様であるが、O_2 系にみられた反応経路の相違による説明は不可能である。$(NO + Ar)^+$ 系の電荷移動反応の特異性は、この系の三重項状態ポテンシャルの NO 分子軸に対する Ar 核の接近方向による異方性に由来している。この説明を裏付けるため行なった非経験的分子軌道計算の結果を図5に示す。Ar の NO 軸方向からの接近時には、NO の

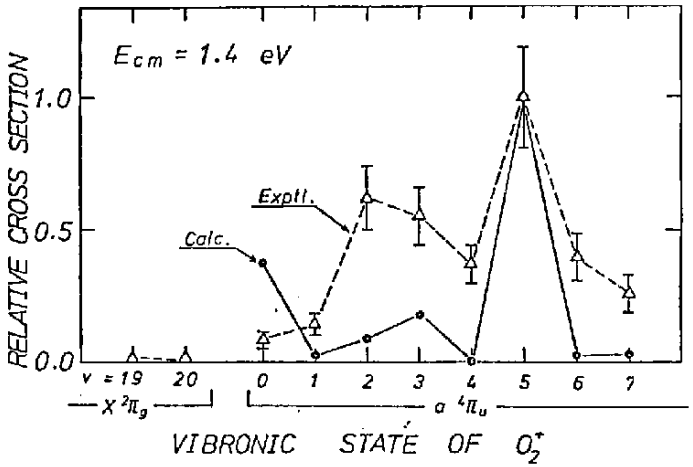

図　3

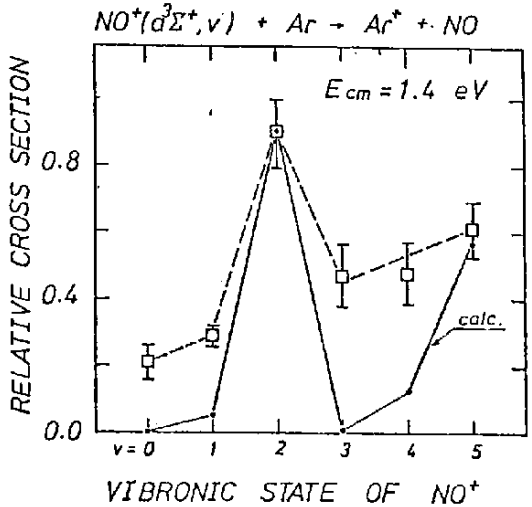

図　4

5 σ軌道と Ar の $3P_z$ 軌道間の交換力のため、Ar^+ + NO 状態と $NO^+(b^3\Pi)$ + Ar 状態が相互作用し、Ar^+ + NO に漸近する状態は安定化して $NO^+(a^3\Sigma^+)$ + Ar に漸近する状態と交差する。電荷移動反応の始状態と終状態は、この交差を通して相互作用する。一方、NO 軸に直角方向からの接近では、NO の1 π軌道と Ar の $3P_x$ 軌道の交換力のため Ar^+ + NO 状態と $NO^+(a^3\Sigma^+)$ + Ar 状態は直接に相互作用する。この様に接近方向により電荷移動反応の始状態と終状態の相互作用の仕方が異なり、それぞれが二つの電荷移動反応機構に対応する。

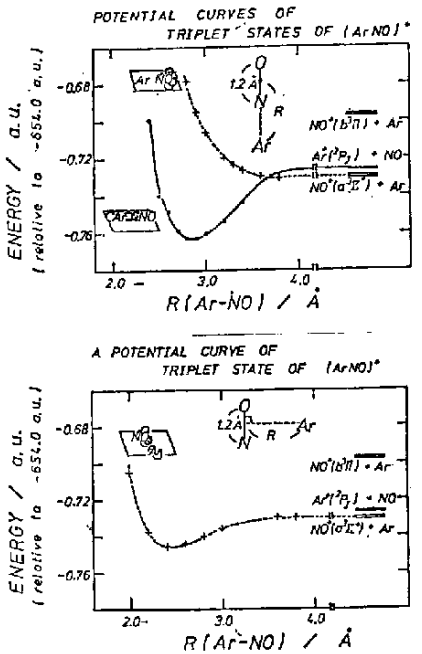

図 5

5．電荷移動反応の二つの機構

電荷移動反応 $BC^+ + Ar \rightleftarrows Ar^+ + BC$ の反応断面積の選別状態依存性を、エネルギー準位差（ΔE）と FC因子を用いたモデル計算と比較した。その結果、現象論的にそれぞれの電荷移動反応を直接機構と複合体機構によるものに分類できた。また、$(H_2 + Ar)^+$、$(O_2 + Ar)^+$、$(NO + Ar)^+$、それぞれの系の反応物が無限遠にある時のポテンシャル図との比較と、対称性に基づく複合体の状態と漸近状態との相関図的な議論より、直接機構と複合体機構をそれぞれ次の様に性格付けできた。直接機構を図6．A に、Ar とBC の接近（座標R）に従がう三枚のBC 核間距離方向（座標r）での断面図として模式的に示す。電荷移動反応の始状態（H_{11}）と終状態（H_{22}）のエネルギー準位が接近する場合、一般に二原子分子BC の核間距離（r）

はイオン化したBC^{+}のそれと異なるため、Ar とBC が無限遠（R ＝∞）にあってもH_{11} とH_{22} はr方向に交差を持つ。R が大きい時には、相互作用はなくエネルギー準位は平行のまま接近してくるが、相互作用領域（R ＝R_c ）に達するとr 方向での交差を通して大きな相互作用が急激に生じて二つのポテンシャルは離れる。R ＝R_c での急激な相互作用で電荷移動が生ずるため、この機構による電荷移動反応はR ＝∞ でのΔE やFC 因子に支配される。一方、図6．B に示す様に始状態（H_{11}）と終状態（H_{22}）がエネルギー的に離れているか、R ＝∞ でr 方向に交差がない場合は、第三の状態（H_{33}）が存在して、まずH_{11} とH_{33} 間の相互作用が大きくH_{11} に漸近する状態が安定化してH_{22} とR 方向で交差を持つ。この交差を通して電荷移動をおこすならば、R ＝∞ でのΔE やFC 因子と反応断面積は無関係となる。この様に複合体機構による電荷移動反応を説明できる。

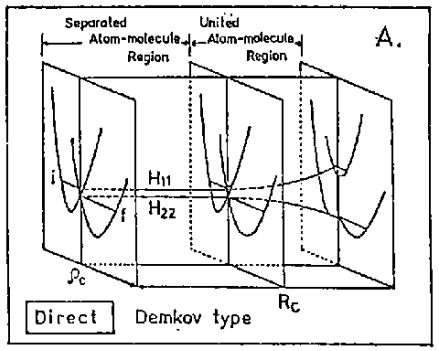

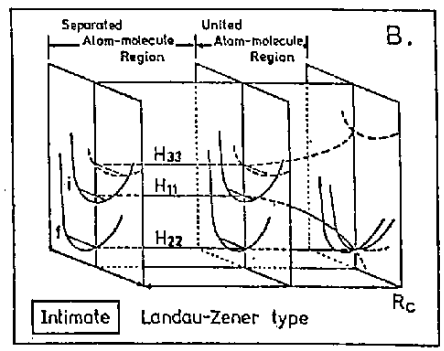

図　6

参考論文要旨

1．可視領域光励起により1,3－シクロヘキサジエン陽イオンラジカルは、トランス－1,3,5－ヘキサトリエン陽イオンラジカルに光異性化する。異性化の過程においてシス－シス－シス型、シス－トランス－シス型、トランス－シス－トランス型の三つのヘキサトリエン陽イオンラジカルも存在し、それぞれの異性体は、類似しているが分離可能な吸収スペクトルを可視と近赤外領域に与える。また、それぞれの陽イオンラジカルの立体構造と光異性化過程を、INDO とCNDO ／S 分子軌道計算により説明できた。

2．有機ハロゲン化物を溶媒とした凍結非晶質溶液のγ－線照射により、芳香族炭化水素、脂肪族アミン、芳香族アミンの陽イオンラジカルが得られた。これらの陽イオンラジカルの電子吸収スペクトルと、親分子の光電子スペクトルを比較し、二つのスペクトルの相関関係を見い出し、お互いに相補的な役割を果たすことが解かった。

3．凍結溶液のγ－線照射による分子間電荷移動により、含窒素芳香族炭化水素化合物のイオンンラジカルを得た。それぞれの陽イオン、陰イオンラジカルを個別に得ることができ、ESR 並びに光吸収分光法を用いて調べた。その結果陽イオンラジカルは、窒素の孤立電子対軌道上にスピン密度の局在した「n 陽イオン」と、π軌道上に非局在した「π陽イオン」に分類することができた。

4．77K と4K における γ - 線照射による凍結トリクロロフルオロメタン溶液中のピリジン陽イオンラジカルの生成を、ESR 並びに光吸収分光法で確認した。陽イオンラジカルは σ 型ラジカルであり、窒素原子の孤立電子対軌道上に正電荷は局在しており、各種重水素化ピリジンを用いてこのことを確認できた。

5．凍結トリクロロフルオロメタン剛体マトリックスの77K における γ - 線照射により、数種のオレフィン類、ジエン類の陽イオンラジカルを得た。ESR スペクトルから陽子による超微細結合定数を決定することができ、それぞれの陽イオンラジカルの電子構造に関する情報が得られた。また、二、三の陽イオンラジカルについて後続の光異性化反応が観測された。

6．反応 $Ar^+ (^2P_J) + H_2 (D_2) \rightarrow ArH^+ (ArD^+) + H (D)$ について反応イオン Ar^+ のスピン - 軌道状態を選別した反応断面積を、TESICO 法を用いて直接測定することができた。その結果、スピン - 軌道状態 $J = 1/2$ からの反応断面積が $J = 3/2$ からのものより大きいことが解かった。

7．反応 $Ar^+ + H_2 (D_2) \rightarrow ArH^+ (ArD^+) + H (D)$ と $Ar^+ + H_2 (D_2) \rightarrow Ar + H_2^+ (D_2^+)$ について、反応イオン Ar^+ のスピン - 軌道状態を選別した反応断面積をTESICO 法

を用いて直接測定した。0.05eV から0.5eV の衝突エネルギーにわたって、反応断面積はスピン- 軌道状態J＝1／2 からのものがJ＝3／2 からのものより大きいことが解かり、反応断面積の比 σ(J＝1／2)／ σ(J＝3／2) はそれぞれのスピン- 軌道状態に含まれる対称性の議論から理解できた。

8． 反応$H_2^+ + Ar \rightarrow ArH^+ + H$ と$H_2^+ + Ar \rightarrow Ar^+ + H_2$ について、反応イオンH_2^+の振動状態を選別した反応断面積をTESICO 法を用いて直接測定した。電荷移動反応については、v＝2 の振動状態で反応断面積の共鳴的な増加がみられた。また、低エネルギー衝突においては陽子移動反応との競争現象が観測された。

9． 等電子的二原子分子N_2 とCO へのAr^+からの電荷移動反応を、Ar^+のスピン- 軌道状態を選別してTESICO 法にて調べた。その結果、反応断面積の状態依存性は二つの分子について異なりそれぞれの反応機構に関連することが解かった。

10． N_2^+イオンからAr への電荷移動反応の反応断面積をN_2^+イオンの振動状態を選別してTESICO 法にて測定した。v＝0 状態からの反応断面積は他の振動状態からのものより小さく、0.3 、1.5 、11.8 eV と衝突エネルギーを上げてもその値は増加しないにもかかわらず、振動エネルギーをv＝1 に上げると反応断面積は急激に増加し、v＝2，3 に従がってゆっく

り増加することが解かった。

11．TESICO 法を電子励起状態イオンの状態選別に応用した。$O_2^+ + H_2 \rightarrow O_2H^+ + H$ と $O_2^+ + H_2 \rightarrow H_2^+ + O_2$ 反応について、O_2^+ イオンの $X^2\Pi_g$ の v＝19，20 と電子励起状態 $a^4\Pi_u$ の v＝0-8 を選別した。その結果、両反応とも電子励起状態からは大きな確率で進み、興味深い振電状態依存性を示すことが解かった。

12．$O_2^+ + HD \rightarrow O_2H^+ (O_2D^+) + D (H)$ 反応において、反応論的同位体効果をTESICO 法にて調べた。同位体効果から、O_2^+ イオンの電子励起状態 $a^4\Pi_u$ からの反応並びに基底状態 $X^2\Pi_g$ の振動励起状態からの反応は直接機構によるものと解かった。

13．電荷移動反応 $NO^+ + Ar \rightarrow Ar^+ + NO$ の反応断面積を、NO^+ の振電状態を選別して TESICO 法にて測定した。その結果、直接機構による反応成分と複合体機構による成分の両方が観測された。また、NO^+ の電子状態 $a^3\Sigma^+$ と $b^3\Pi$ のちがいにより反応断面積が変化することが調べられ、状態の相違により電荷移動に関与する電子の軌道が異なることに由来すると結論付けた。

14．N_2 のしきい電子スペクトルと、N_2^+ から Ar への電荷移動反応過程を利用して、N_2 の

光イオン化効率曲線を解析し、自動イオン化過程を研究した。

15．O_2 の同位体を用いて、光イオン化効率曲線の同位体シフトを解析し、自動イオン化スペクトルの新しい同定を行なった。

主論文

State selected charge transfer reactions in the $BC^+ + Ar$ $BC + Ar^+$ systems : Comparison among BC = H_2, O_2, and NO

Tatsuhisa Kato

Institute for Molecular Science, Myodaiji, Okazaki,
444 Japan

The relative state selected cross sections for the low energy charge transfer (CT) reactions in the systems $H_2^+(X^2\Sigma_g^+,v)$ + Ar, $Ar^+(^2P_J)$ + H_2, $O_2^+(a^4\Pi_u,v)$ + Ar, $Ar^+(^2P_J)$ + O_2, $NO^+(a^3\Sigma^+,v)$ + Ar, and $Ar^+(^2P_J)$ + NO have been determined using the threshold electron-secondary ion coincidence (TESICO) technique. In the $(H_2 + Ar)^+$ system, the cross sections for both the forward and backward reactions were found to show a characteristic internal-state dependence which can be consistently interpreted in terms of a single model based on energy defects (ΔE) and Franck-Condon (FC) factors. In contrast, in the $(O_2 + Ar)^+$ and $(NO + Ar)^+$ systems, the strong dependence of the cross sections on the selected internal states were observed only for the forward (starting from the diatomic ions) reaction, and not for the backward (starting from the Ar^+ ion) reaction. The results for the forward reactions were again interpreted, at least partially, by the energy defects and FC factors between the reactant and product states.

These feautures of the internal-state dependence of cross sections have been discussed in conjunction with the characteristics of the relevant potential energy surfaces of each system. The discrepancy between the $(H_2 + Ar)^+$ system and the $(O_2 + Ar)^+$ and $(NO + Ar)^+$ systems in the behavior of the forward and backward cross sections was ascribed to the difference in the number of potential surfaces involved; in the former system only two surfaces are involved in both forward and backward reactions allowing exactly the same mechanism for both reactions, whereas in the latter two systems, the occurrence of more than two surfaces

causes different mechanisms for the forward and backward reactions. In the $(O_2 + Ar)^+$ system, the doublet and quartet surfaces paticipate in the backward reaction, leading to two different states ($X^2\Pi_g$ and $a^4\Pi_u$) of the O_2^+ product ion, while only quartet surfaces are involved in the forward reaction. In the $(NO + Ar)^+$ system, different reaction paths arize between the $(NO^+(a^3\Sigma^+) + Ar)$ and $(Ar^+ + NO)$ states due to the anisotropy in these interactions. This allows the different behavior of the forward and backward reactions, in spite of the fact that the product state of the backward reaction is predominantly $NO^+(a^3\Sigma^+) + Ar$. An ab initio calculation of partial potential energy surfaces for the triplet states of the $(NO + Ar)^+$ system supported this view.

From these consideration, low-energy charge transfer reactions in the $(BC + Ar)^+$ systems have been classified into two groups according to the possible types of nonadiabatic transitions. These groups are considered to correspond respectively to the phenomenological "direct" and "intimate" reaction mechanisms.

I. INTRODUCTION

Almost all ion-molecule systems $(A + B)^+$ are characterized by at least two close-lying potential energy surfaces corresponding to the two mutually charge-transfered states $A^+ + B$ and $A + B^+$ at large intermolecular distances. The charge transfer (CT) reaction $A^+ + B \rightarrow A + B^+$ is essentially a process of nonadiabatic transitions between these surfaces and thus should be understood in a unified manner as a problem of potential surface interactions. However, very few experimental results have been interpreted from this point of view. For instance, although it has been customary to discuss low-energy charge transfer reactions in terms of "direct" and "intimate" collision mechanisms, almost nothing is known concerning what types of interaction give the "direct" and "intimate" mechanisms. Reactions has just been classified into these two categories according to their phenomenological characteristics, such as angular distribution of reaction products in a crossed beams experiment or collision energy dependence of total cross sections.

On the other hand, high probabilities of many asymmetric charge transfer reactions involving molecules have often been interpreted in terms of the close energy resonance (small energy defect) and favorable Franck-Condon (FC) factors between the reactant and product states.[1-3] However, many other asymmetric charge transfer reactions have also been found not to be interpreted by these factors.[4-7] The energy defects and

FC factors are obviously quantities characterizing the reactants and products at infinite separation, and it is not clear what type of actual interaction yields the cross sections that comply with these quantities at infinite separation.

Studies of internal quantum-state dependence of charge transfer cross sections are particularly suited for the investigation of these problems, because a set of internal states of a reactant provides a set of reaction systems which differ from one another only in energy defects and FC factors. From this standpoint, we have recently studied state-selected charge-transfer reactions in various systems[6-9] using the TESICO technique developed by Koyano and Tanaka.[10] From these studies, we have reached the following conclusion; reactions whose relative cross sections can be simply interpreted by the energy defects and FC factors correspond to the "direct" mechanism and those which can not be interpreted only by these factors correspond to the "intimate" mechanism. The obvious question then is what dynamical factor makes these discrimination.

In order to pursue these questions further, we have studied in the present paper the following state-selected charge-transfer reactions in the $(BC + Ar)^+$ systems.

$$H_2^+(X^2\Sigma_g^+,v) + Ar \rightarrow Ar^+ + H_2 \qquad (1)$$

$$Ar^+(^2P_J) + H_2 \rightarrow H_2^+ + Ar \qquad (2)$$

$$O_2^+(X^2\Pi_g,v;a^4\Pi_u,v) + Ar \rightarrow Ar^+ + O_2 \qquad (3)$$

$$Ar^+(^2P_J) + O_2 \rightarrow O_2^+ + Ar \qquad (4)$$

$$NO^+(a^3\Sigma^+, v) + Ar \rightarrow Ar^+ + NO \qquad (5)$$

$$Ar^+(^2P_J) + NO \rightarrow NO^+ + Ar \qquad (6)$$

The internal states selected were v=0-4 for reaction (1), $X^2\Pi_g$, v=19 and 20 and $a^4\Pi_u$, v= 0-7 for reaction (3), and v=0-5 for reaction (5). For reactions (2), (4), and (6), the selected states were spin-orbit states (J=1/2 and J=3/2) of the Ar^+ ion. From the detailed comparison of these experimental results in conjunction with the characteristics of the potential energy curves for the diatomic species BC and BC^+ [at infinite intermolecular separation between $Ar(Ar^+)$ and $BC^+(BC)$], we propose two distinct types of potential surface interactions (transitions) responsible for the charge transfer reactions in the $(BC + Ar)^+$ systems. These are a "Landau-Zener type"[11] interaction in which the transition occurs at an avoided crossing point of potential curves along the intermolecular distance between Ar and BC, and a "Demkov type"[11] interaction in which the transition occurs by a sharp increase in coupling matrix elememts between two potential surfaces with the approach of two reagents. The latter type of transition, which takes place without potential crossings along the radial coordinate between Ar and BC, are considered to be caused by the coupling with the vibrational motion of BC. Otherwise, the probability of such a transition would be extremely small at such low collision energies as used in the present experiments. These two types of interaction mechanisms are considered to correspond respectively to the "intimate" and "direct" reaction

mechanisms. For the case of the $(Ar + NO)^+$ system, we have also performed an ab initio calculation of the partial potential energy surfaces, with the results which support the above view.

The $(H_2 + Ar)^+$ system is the one in whish CT reactions have been studied most extensively. Previous state selected studies[2,3(b),8] have shown that reaction (1) complies with a model based on the energy defects and FC factors. Crossed beams studies have also been performed[12] with the results which are in good agreement with that of the state selected studies. Reaction (2) has also been shown to proceed via a direct mechanism in a crossed beams studies.[13] Detailed theoretical studies[14] are available for reaction (2) with emphasis on its relation to the proton transfer reaction $Ar^+ + H_2 \rightarrow ArH^+ + H$. For the present analysis, we adopted our previous data[8] for reaction (1), and new coincidence measurements were performed for reaction (2).

Concerning the $(O_2 + Ar)^+$ system, on the other hand, an evidence for the CT reaction via an intimate collision mechanism has been presented in reaction (4) by Mauclaire et al.[4] using ICR. They concluded that the state of the O_2^+ product ion in the reaction $Ar^+(^2P_{3/2}) + O_2 \rightarrow O_2^+ + Ar$ is $X^2\Pi_g$, v=9, which lies much lower than the states in resonance with the reactant state, such as $X^2\Pi_g$, v=19, or $a^4\Pi_u$, v=0. Kobayashi et al.[5] also proposed an intimate collision mechanism, in interpreting the result of their absolute cross section measurements. In this mechanism, they suggested the possibility of an inner-shell level mixing

during collisions.

For the $(NO + Ar)^+$ system, the large CT cross sections for both reactions (5) and (6) have been attributed to the close energy resonance between the recombination energy of Ar^+ and the level of $NO^+(a^3\Sigma^+)$. In fact, a resonance-like enhancement of the cross section for reaction (5) has been observed at v=2 in our state selected measurement,[9] in agreement with the prediction from the energy defects and FC factors. Also the state of the NO^+ product ion of reaction (6) has been shown to be $a^3\Sigma^+$, $v\simeq 0$ by Mauclaire et al.[4] On the basis of these results, both reactions (5) and (6) have been considered to proceed by a direct mechanism ; however, it should also be noted that several evidences for the formation of a collision complex have been reported for reaction (6). Herman et al.[15] estimated, in a crossed beams experiment, the relative importance of the direct and complex mechanisms for reaction (6) and concluded that the intermediate complex formation becomes increasingly more important as collision energy is decreased. Kobayashi et al.[5] have shown that the CT cross section of reaction (6) exhibits a minimum as a function of collision energy, and that the lower energy part of the curve obey the $E^{1/2}$ dependence. The result of the collision energy dependence seems to suggest the occurrence of a change in the reaction mechanism as the collision energy is varied.

II. EXPERIMENTAL.

The threshold electron-secondary ion coincidence (TESICO) technique and the apparatus TEPSICO have been described in detail elsewhere.[10] Briefly, the apparatus consists of a helium Hopfield continuum light source, a 1 m Seya-Namioka monochromator, an ionization chamber, a reaction chamber, a hemispherical electron energy analyzer, and a quadrupole mass spectrometer, these being assembled together via a six-stage differential pumping system. The reactant ions are produced by photoionization of parent molecules at the threshold wavelength for each internal state of interest. The ions produced in the ionization chamber are extracted, formed into a beam of desired velocty, and injected into the reaction chamber filled with a neutral reagent. The product ions produced there, as well as unreacted primary ions, are extracted from the chamber, mass-analyzed, and counted in coincidence with the threshold electron signals obtained on the opposite side of the ionization chamber. Coincidence measurements were performed by feeding the threshold photoelectron and the mass-analyzed ion signals into the start and stop input, respectively, of a time-to-pulse height converter and analyzing the resulting output signals by a multichannel pulse height analyzer. The raw data obtained are thus the coincidence TOF spectra for the primary and secondary ions. From the ratios of the integrated intensities of these primary and secondary ion peaks, the relative reaction cross sections for individual states are obtained directly.

High purity sample gasses were obtained from Japan Oxygen Co. and used without further purification. The nominal purities of these gasses are 99.9999% for hydrogen, 99.99% for oxgen, 99.15% for nitric oxide, and higher than 99.999% for argon.

III. RESULTS

Experimental results are summarized in Figs.1-4. For reactions (1), (3), and (5), the relative cross sections are plotted as a function of the vibrational quantum state selected (Figs.1-3), while for reactions (2), (4), and (6), the ratios of the cross sections for the two selected (spin-orbit) states are plotted vs collision energies (Fig.4).

Figure 1 shows the relative cross sections of reaction (1) for v=0-4 of the $H_2^+(X^2\Sigma_g^+)$ ion, determined at collision energies of 0.77 and 19.0 eV.[8] Notable features pertaining to this reaction are summarized as follows. The cross sections for v=0 and 1, which are extremely small at 0.77 eV of collision energy because of the endoergicity of reaction (1) for these vibrational states, are considerably enhanced when collision energy is increased to 19 eV. The enhancement is particularly prominent for v=1. A resonance-like peak in the relative cross section is observed at v=2, at both collision energies. This peak, however, looks less conspicuous at high collision energies than at low collision energies due to the above-mentioned large enhancement of the v=1 cross section. The enhancement of cross sections at v=2 is interpreted as due to the close energy resonance between the $H_2^+(v=2)$ + Ar and $Ar^+(^2P_{1/2})$ + $H_2(v=0)$ states, as shown in Fig.5. The manifestation of this resonance is also found in the result of reaction (2), shown in Fig.4. The ratios of the cross sections for the two spin-orbit states of Ar^+(J=1/2 and 3/2) are found to be very large; 10.1±2.3 and 5.9±1.3 at collision energies of

0.2 and 1.4 eV respectively.

Experimental results for reaction (3) are shown in Fig.2. The two curves correspond to two different collision energies (1.4 and 5.8 eV) and are normalized at v=5 of the $a^4\Pi_u$ state. Several interesting feautures are clearly seen from the figure. The cross sections for reaction (3) are extremely small for the v=19 and v=20 states of $X^2\Pi_g$ despite the fact that reaction (3) is exoergic for v=19 of $X^2\Pi_g$ and above, while the cross sections become significant at v=0 of the $a^4\Pi_u$ state which lies only 0.17 eV above the $X^2\Pi_g$,v=20 state. When vibrational quantum number is increased in the $a^4\Pi_u$ state, a sharp rise in the cross section is observed at v=2, followed by a gradual decrese except at v=5 , where the cross sections show a resonance-like enhancement. This characteristic enhancement is also attributable to the close energy resonance between the $O_2^+(a^4\Pi_u, v=5) + Ar$ and $Ar^+(J=3/2) + O_2(v=5)$ states.

Figure 3 shows similar results for reaction (5) at a collision energy of 1.4 eV. Reaction (5) is slightly (by 0.09 eV) endoergic for v=0 of the $a^3\Sigma^+$ state of NO^+ and exoergic for v=1 and above. Here again, a pronounced resonance-like enhancement of the cross section is observed at v=2 of the $a^3\Sigma^+$ state. Except this point, the cross section shows a tendency to increase slightly but steadily with increasing v in the $a^3\Sigma^+$ state. It is notable that the substantial cross section is observed at v=0 in spite of the fact that reaction (5)

is endoergic by 0.1 eV for v=0. Undoubtedly the reaction was caused by the collision energy of 1.4 eV.

In contrast to the above reactions which showed pronounced enhancement of cross sections at a particular selected level, reactions (4) and (6) show only very weak dependence of cross sections on selected internal states. The ratios (r) of the J=3/2 and J=1/2 cross sections are essentially unity at all collision energies studied; r=1.0±0.3 and 1.2±0.2 at 1.4 and 5.8 eV, respectively, for reaction (4), and 0.9±0.1 , 1.4±0.2, and 1.1±0.2 at 0.2, 1.4, and 5.8 eV, respectively, for reaction(6).

IV. DISCUSSIONS

A. Comparison with Model Calculation and Consideration of Potential Energy Surfaces.

The state selected (relative) cross sections obtained were compared with the results of a model calculation based on the energy defects (ΔE) and FC factors. Since these factors are considered to have significance only in the "direct" type reactions and not in the "intimate" type reactions, the comparison of the calculated and experimental results is expected to give information on the reaction mechanism.

The detailed procedure for the model calculation is described elsewhere[6,9]. The model is based on the assumption that each product state can be treated independently as a two-state problem to which the impact paremeter theory of Rapp and Francis[16] can be applied. The cross sections for each specific pair of the reactant and product states of $BC^+(v) + Ar \rightarrow BC(v') + Ar^+(^2P_J)$ or $Ar^+(^2P_J) + BC(v=0) \rightarrow Ar + BC^+(v')$ are first calculated according to the Rapp and Francis formula. The charge transfer cross sections for each selected initial state $\sigma(i)$ are then obtained by summing up the contribution from each product state with the weight of the FC factors. The summation is taken over all energetically attainable product states for a given collision energy. The Rapp and Francis cross section as a function of ΔE has a very sharp

peak around $\Delta E=0$, and thus the contribution to $\sigma(i)$ essentially comes from only a few product states with small ΔE.

i. $(H_2 + Ar)^+$ system

The comparison between the experimental and calculated relative cross sections of reaction (1) is shown in Fig.6. Feautures of the experimental results pointed out above are seen to be well reproduced by the calculation; the substantial increase in the relative cross section for v=0 and 1 at the higher collision energy is beautifully reproduced. Furthermore the claculation confirms that the resonsnce-like enhancement of the relative cross section at v=2 is indeed due to the close energy resonance between the $H_2^+(v=2)$ + Ar and $Ar^+(^2P_{1/2})$ + $H_2(v=0)$ states. Similar comparison for reaction (2) is given in Fig.4 (left panel). The ratio of the cross sections $\sigma(1/2)/\sigma(3/2)$, which is much larger than unity, and its variation with collision energy are again satisfactorily reproduced by the calculation. The enhanced J=1/2 cross section compared with that of J=3/2 is also attributed to the above resonance.

The potential energy surfaces of the relevant states at infinite intermolecular distance between Ar and H_2 are shown in Fig.5. Obviously these correspond to the diatomic potential curves of $H_2(X^1\Sigma_g^+)$ [shifted vertically by the magnitudes of ionization potentials for $Ar^+(^2P_{3/2})$ and $Ar^+(^2P_{1/2})$] and $H_2^+(^2\Sigma_g^+)$. The charge transfer reactions (1) and (2) are eventually the transitions between one of the solid line curves and

the dotted line curve. When Ar and H_2 are brought together to form a linear complex, the asymptotic $Ar^+(^2P)$ + $H_2(X^1\Sigma_g^+)$ and $H_2^+(X^2\Sigma_g^+)$ + Ar states give rise to the $^2\Sigma$, $^2\Pi$, and $^2\Pi$ and $^2\Sigma$ molecular states, respectively[17]. As Ar and H_2 approach each other, the two $^2\Sigma$ states begin to interact and the potential curves which are crossed by each other at infinite separation become separated. Two potential curves remain almost parallel until the system reaches the region of strong interaction where the transition takes place. Since this region in general would occur at comparatively large intermolecular distances for the potential situation as in Fig.5, the transition probability in this type of interaction would be governed by the asymptotic properties such as energy defects and the FC factors between the reactant and product states, explaining the experimental results. We call this type of transition a "Demkov type transition" in this paper. This reaction mechanism will be discussed further in Section C. The $(H_2 + Ar)^+$ system is considered to be a typical example of systems in which CT proceeds via a Demkov type transition in both ways.

ii. $(O_2 + Ar)^+$ system

In the case of the $(O_2 + Ar)^+$ system, five electronic states are considered to be involved in the processes of reactions (3) and (4). The potential energy surfaces of these states at infinite intermolecular separation between Ar and O_2 are shown in Fig.7. However, the model calculations for reactions (3) and (4) were performed by taking only the

transition between the levels of the $O_2^+(a^4\Pi_u)$ + Ar and $Ar^+(^2P_J)$ + O_2 states into consideration, because it is known that the contribution to the calculated cross sections essentially comes from only a few product states with the smallest energy defects.

The calculated results are shown in Fig.8 (solid line curve), together with the experimental results (broken line curve) at a collision energy of 1.4 eV. It is seen that the essential features of the experimental cross sections for the $a^4\Pi_u$ state are reproduced fairly well by the calculation, except at v=0. [The disagreement at v=0 might be caused by the following reason; under our experimental conditions, the v=21 state of $O_2^+(X^2\Pi_g)$ were not resolved from the v=0 state of $O_2^+(a^4\Pi_u)$ and gave threshold electrons of comparable intensity as that of the latter state. Thus the apparent cross sections were reduced by the effect of the unreactive $O_2^+(X^2\Pi_g, v=21)$ state.] The fact that the model calculation reproduces the experimental results fairly well leads to the conclusion that reaction (3) with $O_2^+(a^4\Pi_u)$ proceeds, predominantly at least, via a direct interaction between the $O_2^+(a^4\Pi_u)$ + Ar and $Ar^+(^2P_J)$ + O_2 states. The extremely small cross sections for the v=19 and 20 states of $O_2^+(X^2\Pi_g)$ are attributed to the very small FC factors ($<10^{-22}$) between these states and the v=0 and 1 states of $O_2(X^3\Sigma_g^-)$, the latter states being the two energetically favorable states of the product molecule. This fact may suggest that the reaction (3) with $O_2^+(X^2\Pi_g)$ also proceeds by a direct mechanism.

In contrast to the results for reaction (3), no significant difference is observed in the cross section of reaction (4) between the two spin-orbit states; the experimental results show that the ratios of the J=3/2 and J=1/2 cross sections are essentially unity at both collision energies studied (1.4 and 5.8 eV), as shown in Fig.4 (middle panel). If the microscopic reaction paths of this reaction are the same as that of reaction (3), the cross section of the $Ar^+(J=1/2) + O_2(v=0)$ state, which lies closer to the levels of $O_2^+(a^4\Pi_u,v) + Ar$ than the $Ar^+(J=3/2) + O_2(v=0)$ state, is expected to be larger than that of the latter state (due to smaller ΔE), as is also predicted by the model calculation (solid line curve in Fig.4). Thus the above result suggests that in reaction (4) the charge transfer does not occur by a simple electron jump mechanism to form $O_2^+(a^4\Pi_u)$, but proceeds via some complex states, probably to form $O_2^+(X^2\Pi_g)$. As described in Introduction, such a mechanism for reaction (4) has previously been proposed by Kobayashi et al.[5], and an evidence for this mechanism has been presented by Mauclaire et al.[4] in an ICR experiment.

From all these evidences, it seems certain that the predominant microscopic reaction paths are different for reaction (3) and (4) in the collision energy range studied; reaction (3) with $O_2^+(a^4\Pi_u)$ proceeds via a direct mechanism to form $Ar^+(^2P_J) + O_2$, while the reverse CT process [reaction (4)] proceeds via a complex mechanism to form $O_2^+(X^2\Pi_g) + Ar$, rather than $O_2^+(a^4\Pi_u) + Ar$. Considering the formation of united ion-molecules of a linear geometry, two quartet [$^4\Pi$

(doubly degenerate) and $^4\Sigma$] and two doublet [$^2\Pi$ (doubly degenerate) and $^2\Sigma$] states are possible to be formed from the combination of $Ar^+(^2P) + O_2(X^3\Sigma_g^-)$. On the other hand, from the combinations of $O_2^+(X^2\Pi_g) + Ar$, $O_2^+(a^4\Pi_u) + Ar$, and $O_2^+(A^2\Pi_u) + Ar$, only $^2\Pi$, $^4\Pi$, and $^2\Pi$ states, respectively, can be formed[17]. Starting from the $O_2^+(a^4\Pi_u) + Ar$ state, reaction (3) can proceed only along a path on the quartet potential surface, and thus CT must take place through a transition from this surface to another $^4\Pi$ surface correlating to $Ar^+(^2P) + O_2(X^3\Sigma_g^-)$. Considering the above results that the experimental state-dependence of the cross section is interpreted by the energy defects and FC factors, the two $^4\Pi$ potential surfaces must be cupled directly to give a Demkov type transition, just as in reaction (1) and (2). Charge transfer through this transition seems to be the predominant mechanism for reaction (3). For reaction (4), on the other hand, two different paths are posible, one on the doublet potential surfaces and the other on the quartet potential surfaces. The path on the quartet potential surfaces should be exactly the reverse of the path of reaction (3). However the above comparison between the experimental and calculated results has shown that this path is not the one through which the reaction proceeds predominantly. As to the doublet path, the three potential surfaces with the same Π symmetry seems to be involved, one correlating to $O_2^+(A^2\Pi_u) + Ar$, one correlating to $O_2^+(X^2\Pi_g) + Ar$, and the other correlating to $Ar^+(^2P_J) + O_2$. Among them, the two $^2\Pi$ state correlating to $O_2^+(A^2\Pi_u) + Ar$ and $Ar^+(^2P_J) + O_2$ lie much closer to each other, as can be seen from Fig.7. As

reactants approach each other the asymptotic $Ar^+(^2P_J)$ + O_2 potentials are increasingly stabilized by the interaction between these two $^2\Pi$ states, until they experience an avoided crossing with the lower lying $^2\Pi$ potential correlating to $O_2^+(X^2\Pi_g)$ + Ar. Reaction (4) is considered to proceed through a non-adiabatic transition at this avoided crossing. Since this type of crossing would generally occur at very short intermolecular distances where the potential energy surfaces at infinite separation are completely distorted, the energy defects and FC factors at infinite separation would not be reflected in the transition probability, in agreement with the experimental results. We call this type of transition a "Landau-Zener type" transition, which is also discussed further in Section C.

iii. $(NO + Ar)^+$ system

As mentioned in Introduction, the large CT cross sections have been attributed to the close energy resonance between the recombination energy of Ar^+ and the levels of $NO^+(a^3\Sigma^+)$.[5] In fact experimental evidence has shown that reaction (6) occurs predominantly to form the product NO^+ ion in the $a^3\Sigma^+$ state[4]. While it has been shown in this way that reaction (5) and (6) are CT reactions between two resonantly lying states, some evidences of complex formation have also been presented. For instance, Herman et al.[15] have reported that the intermediate complex formation becomes increasingly more important as collision energy is lowered in reaction (6). Comparing the relative cross sections for reaction (5)

with the results of model calculation, we find in the present study that not only a direct collision mechanism but also an intimate collision mechanism is involved in reaction (5), as described below.

Figure 9 compares the relative cross sections for reaction (5) with the results of the model calculation. One can see that while the two features of the experimental results, i.e., the resonant enhancement of the cross section at v=2 and the increase in the cross section with increasing vibrational quantum number between v=0 and 1 and v=3 and 5, are well reproduced by the model calculation, there exist discrepancies between the two results concerning the relative magnitudes of the cross sections. In particular, it is to be noted that the experiment gives cross sections of substantial magnitude at v=0 and 3 where the calculation predicts cross sections of essentially zero when both results are normalized at v=2. The gross agreement between the experimental and calculated results would probably indicate that reaction (5) proceeds, at least to some extent, by an electron jump mechanism at large intermolecular separation. At the same time, however, the fact that the relative cross sections at some vibrational states are considerably larger than those predicted by the model calculation would indicate that a complex mechanism is also operative in this reaction. In other words, the cross section for reaction (5) at this collision energy is interpreted as consisting of two components, one whose vibrational-state dependence is determined simply by the energy defects and FC factors, and the other whose vibrational-state dependence is not simply determined by

these factors. The nature of these two mechanisms are discussed in Section B.

In contrast to the results of reaction (5), the close energy resonance between the $Ar^+(^2P_{1/2})$ + NO(v=0) and $NO^+(a^3\Sigma^+,v=2)$ + Ar states was not manifested at all in the cross sections of reaction (6). Namely the rations of the relative cross sections for $Ar^+(^2P_{1/2})$ and $Ar^+(^2P_{3/2})$ were found to be unity within the experimental error, in spite of the fact that the model calculation predicted large values for this ratio, as shown in Fig.4 (right panel). Since it has been shown that the product state of reaction (6) is $NO^+(a^3\Sigma^+)$ + Ar,[4] reaction (6) must be considered as the reverse reaction of reaction (5). Considering this fact, the absence of an enhanced J=1/2 cross section in reaction (6) is a peculiar result. It can not be interpreted by the difference in the reaction paths, as was done in the case of the $(Ar + O_2)^+$ system. This problem is also discussed in the next section based on the results of ab initio calculation.

B. Ab initio MO calculation

In order to better understand the above experimental results, we have performed some ab initio MO calculations of the partial potential energy surfaces of these reaction systems. Here, we present the results on the $(NO + Ar)^+$ system.

Before presenting the results of calculation, a brief discussion of the symmetry properties of the relevant complex states would be appropriate. From the consideration of molecular orbital symmetries, twelve complex states are expected to evolve from the $Ar^+(^2P)$ + $NO(X^2\Pi)$ inetraction,[17] without considering the spin-orbit interactions in both Ar^+ and NO. Of these, however, only a few states are considered to be involved in reactions (5) and (6). First of all, as it has been shown that the main product state of reaction (6) is $NO^+(a^3\Sigma^+)$ + Ar, only triplet potential surfaces would need to be considered as the paths of reaction (5) and (6). Furthermore, since the $NO^+(a^3\Sigma^+)$ + Ar and $NO^+(b^3\Pi)$ + Ar states are the two triplet states lying much closer to the $Ar^+(^2P)$ + NO state than any other triplet state (see Fig.10), consideration of only these two states as partners of the CT interaction of the Ar^+ + NO state will suffice for the present purpose.

The electronic configurations of $NO^+(a^3\Sigma^+)$, $NO^+(b^3\Pi)$, and $NO(X^2\Pi)$ are $\cdots(1\pi)^1(5\sigma)^2(2\pi)^1$, $\cdots(1\pi)^2(5\sigma)^1(2\pi)^1$, and $\cdots(1\pi)^2(5\sigma)^2(2\pi)^1$, respectively. Thus, if an electron is transferred from the 1π orbital of NO to Ar^+, the Ar + $NO^+(a^3\Sigma^+)$ state would be formed, whereas if an electron is transferred from the 5σ orbital of NO to Ar^+, the Ar + $NO^+(b^3\Pi)$ state would be formed. Since these two orbitals (1π and 5σ) respectively extend in the directions perpendicular and along the internuclear axis of NO, the broad-side and head-on approach of Ar^+(Ar) to NO(NO^+) would lead to different exchange interactions between the reactants; in the former

approach the interaction between the 3p orbital of Ar and 1π orbital of NO is favored and in the latter approach the interaction between the 3p orbital of Ar and the 5σ orbital of NO is favored. The former interaction yields A' complex state in which the asymptotic $Ar^+(^2P)$ + $NO(X^2\Pi)$ and $NO^+(a^3\Sigma^+)$ + Ar states are mixed and the latter interaction yields A' and A'' complex states in which the asymptotic $Ar^+(^2P)$ + $NO(X^2\Pi)$ and $NO^+(b^3\Pi)$ + Ar states are mixed. The formation of these two different complex states would probably explain the salient feautures observed in reactions (5) and (6).

The calculation was performed by an open-shell SCF method without configuration interaction using the Huzinaga's MIDI-4 basis sets (GTO's)[18]. Figure 11 shows the calculated potential energies for the triplet ground state (A') as a function of the angle Θ the line of centers of the collision makes with the internuclear axis of NO. (For Θ=0, see the inset.) The bond length r(N-O) and the distance R between the center-of-mass of NO and Ar were fixed at 1.2 A and 2.8 A, respectively. It is seen that the curve consists of two characteristic regions, one corresponding to the angles of broad-side collisions (indicated by broken line ---+---), and the other corresponding to the angles of head-on collisions (indicated by solid line ——•——). The former region of the potential surface (broken line curve) is shown in Fig.12 as a function of the distance R. The bond length r(N-O) and angle Θ are now fixed at 1.2 A and 90, respectively. Based on the analysis of the calculated positive charge distribution and the nature of the

molecular orbitals involved, it turned out that this curve asymptotically correlates to the $NO^+(a^3\Sigma^+)$ + Ar state, as shown in Fig.12. This state is stabilized as R is decreased, due to the CT interaction between the $NO^+(a^3\Sigma^+)$ + Ar and $Ar^+(^2P)$ + NO states.

On the other hand, the collinear region (Θ=180) of the potential surface (solid line curve) is shown in Fig.13 as a function of R at the same fixed r(N-O) of 1.2A. From the same analysis, it was found that the surface now asymptotically correlates to the $Ar^+(^2P)$ + NO state and is stabilized as R is decreased by the CT interaction between the $Ar^+(^2P)$ + NO and $NO^+(b^3\Pi)$ + Ar states. In the collinear approach, the solid line curve corresponds to a Π state and undergoes a crossing with the unstabilized Σ state which asymptotically correlates to the $NO^+(a^3\Sigma^+)$ + Ar state (broken line curve).

Thus the calculated results indicate that two mechanisms are indeed possible for the CT reactions (5) and (6). In the broad-side approach, the two asymptotic states $NO^+(a^3\Sigma^+)$ + Ar and $Ar^+(^2P)$ + NO are directly coupled. In this case, a direct type transition is expected between the two states. In the case of the collinear approach, on the other hand, the asymptotic $Ar^+(^2P)$ + NO state is first stabilized by the CT interaction with the $NO^+(b^3\Pi)$ + Ar state (interaction between the 5σ orbital of NO and the $3p_z$ orbital of Ar), and then makes an avoided crossing with the $NO^+(a^3\Sigma^+)$ + Ar state at much shorter intermolecular distances. The transition takes place at this avoided crossing. This

interaction seems to give the intimate type collision mechanism. These two interaction mechanisms seem to correspond to the two components of the experimental cross section for reaction (5). The relative importance of the two mechanisms would be different between reaction (5) which starts from the $NO^+(a^3\Sigma^+)$ + Ar state and reaction (6) which starts from the $Ar^+(^2P)$ + NO state. This difference probably gives rise to the different appearance of the state-dependence of the experimental cross sections between reactions (5) and (6).

C. Two types of collision mechanism.

As mentioned in Introduction, one of our purpose in the present study is to clarify as far as possible the nature of the two types of mechanism for charge transfer reactions in the $(BC + Ar)^+$ systems, i.e., the "direct" and "intimate" reaction mechanisms. Although many investigators have discussed low-energy charge transfer reactions in terms of these two mechanisms, the detailed nature of these mechanisms have been largely unknown.

In this section, we propose, summarizing the above discussion, two distinct types of potential surface interactions in the $(BC + Ar)^+$ systems. We believe that these two interaction mechanisms correspond to the two phenomenological reaction mechanisms. The conclusion has been reached from the consideration of the experimental results in conjunction with the situation of the relevant potential energy curves of the

reactant and product states at infinite intermolecular separation, as well as with the results of the ab initio calculation for the $(NO + Ar)^+$ system.

Figure 14 shows the two proposed types of interaction mechanisms schematically. In each type, three cuts of the potential energy surfaces along the r(B-C) coordinate are shown. The potential energy surfaces for a system in which CT reaction is considered to proceed via a direct mechanism are shown in Fig.14(A). In such a system, Ar and BC have similar ionization potentials and thus the electronic states of the $Ar^+ + BC$ and $Ar + BC^+$ systems lie very close to each other. Since the equilibrium internuclear distance of a diatomic system is generally different between the neutral and ionic species, the potential energy surfaces of the two electronic states cross at infinite intermolecular separation between Ar and BC. The mixing between the two CT states around the crossing point is negligible at large intermolecular separation. As Ar and BC approach each other, the mixing of these states becomes significant and the crossing becomes avoided, as shown in the middle cut. However, the two potential surfaces corresponding to the initial and final states [H_{11} and H_{22} in Fig.14(A), respectively] remain almost parallel, being separated by the energy defect ΔE, until the system reaches the region of strong interaction. When this region is reached, the interaction suddenly gets strong and the predominant transition between H_{11} and H_{22} takes place here. This region is considered to lie around the boundary between the separated and united

atom-molecule regions and is expected to be at fairly large intermolecular distances R. The probability for this transition is expected to be governed by the energy defects and FC factors between the reactant and product states at infinite separation, because of the above-mentioned parallelness of the potential surfaces, providing the appearance of the "direct" reactions. Although the transitions are indeed induced by the collisions between Ar and BC, apparently no crossings of potential surfaces occur along the R(Ar-BC) coordinate. The transition is evidently caused by the avoided crossing along the r(B-C) coordinate. In this context, we call this type of charge transfer mechanism "Demkov type" mechanism. Reactions (1)-(3) and a part of reaction (5) (broad-side approach) seem to belong to this mechanism.

If the potential energy surfaces of the initial and final states lie comparatively far from each other and thus have no crossing along the r(B-C) coordinate at infinite R(Ar-BC), as shown in Fig.14(B), the interaction between the two electronic states would be so small even at the boundaries of the separated and united atom regions that a direct type (Demkov type) transition cannot take place. In such a situation, if a third state (H_{33}) lies closely above the initial state (H_{11}), it could happen that the interaction between these two electronic states lowers the initial state considerably as R(Ar-BC) is decreased, eventually causing an avoided crossing with the low lying final state (H_{22}). The charge transfer rections can proceed via transitions between the H_{11} and H_{22} surfaces at this avoided crossing. Since this type of crossing would

generally occur at very small intermolecular distances R(Ar-BC) deep in the united atom-molecule region, where the properties of the reactants at infinite separation are completely lost, the transition probability at this crossing would not reflect such properties as the FC factors and energy defects. This type of mechanism seems to correspond to the "intimate" or "complex" collision mechanism. We call this type of charge transfer mechanism "Landau-Zener type" mechanism in the context that the charge transfer takes place via surface transitions at an avoided crossing along the collision coordinate [R(Ar-BC)]. Reaction (4) and a part of reaction (5) (head-on approach) are the examples of reactions which proceed by this mechanism.

V. ACKOWLEDGMENTS

The author wishes to express his profound gratitude to Professor Inosuke Koyano for his helpful guidance and generous encouragement. The author thanks Dr. Kenichiro Tanaka for his helpful direction, collaboration and exciting discussions troughout this work. The author is much indebted to Dr. Shigeki Kato for his help with the ab initio calculation and for valuable discussions. The calculations of the FC factors and the Rapp and Francis cross sections, as well as the ab initio MO calculations have been carried out at the computer center of the Institute for Molecular Science.

REFFERENCES.

1. See, for example, (a) J. B. Laudenslager, W. T. Huntress, Jr., and M. T. Bowers, J. Chem. Phys. 61, 4600 (1974) and references cited therein; (b) J. Durup, in Interaction Between Ions and Molecules, edited by P. Ausloos (Plenum, New York, 1975), p.619 and references cited therein; (c) R. Marx, in Kinetics of Ion Molecule Reactions, edited by P. Ausloos (Plenum, New York, 1978), p.103 and references cited therein.

2. (a) F. M. Campbell, R. Browning, and C. J. Latimer, J. Phys. B 13, 4257 (1980); (b) B 14, 3493 (1981).

3. (a) S. L. Anderson, F. A. Houle, D. Gerlich, and Y. T. Lee, J. Chem. Phys. 75, 2153 (1981); (b) F. A. Houle, S. L. Anderson, D. Gerlich, T. Turner, and Y. T. Lee, ibid. 77, 748 (1982); (c) S. L. Anderson, T. Turner, B. H. Mahan, and Y. T. Lee, ibid. 77, 1842 (1982).

4. R. Marx, G. Mauclaire, and R. Derai, Int. J. Mass Spectrom. Ion Phys. 47, 155 (1983).

5. (a) N. Kobayashi, J. Phys. Soc. Japan 36, 259 (1974); (b) N. Kobayashi, Y. Kaneko, F. Koike, and T. Watanabe, ibid. 42, 1701 (1977).

6. T. Kato, K. Tanaka, and I. Koyano, J. Chem. Phys. 77, 834 (1982).

7. T. Kato, K. Tanaka, and I. Koyano, J. Chem. Phys. 77, 337 (1982).

8. K. Tanaka, T. Kato, and I. Koyano, J. Chem. Phys. 75, 4941 (1981).

9. T. Kato, K. Tanaka, and I. Koyano, J. Chem. Phys. 79, 5969 (1983).

10. (a) K. Tanaka and I. Koyano, J. Chem. Phys. 69, 3422 (1978); (b) I. Koyano and K. Tanaka, ibid. 72, 4858 (1980).

11. M. S. Child, Atom-Molecule Collision Theory, edited by R.B.

Bernstein (Plenum, New York, 1979), p.427.

12. R. M. Bilotta, F. N. Preuninger, and J. M. Farrar, Chem. Phys. Lett. 74, 95 (1980).

13. P. M. Hierl, V. Pacak, and Z. Herman, J. Chem. Phys. 67, 2678 (1977)

14. (a) P. J. Kuntz and A. C. Roach, J. Chem. Soc. Faraday Trams.2 68, 259 (1972); (b) S. Chapman and R. K. Preston, J. Chem. Phys. 60, 650 (1974); (c) M. Baer, Mol. Phys. 35, 1637 (1978); (d) M. Baer and J. A. Beswick, Chem. Phys. Lett. 51, 360 (1977); (e) Phys. Rev. A19, 1559 (1979).

15. Z. Herman, V. Pacak, A. J. Yencha, and J. Futrell, Chem. Phys. Lett. 37, 329 (1975).

16. D. Rapp and W. E. Francis, J. Chem. Phys. 37, 2631 (1962).

17. G. Herzberg, Molecular Spectra and Molecular Structure. III Electronic Spectra and Electronic Structure of Polyatomic Molecules (Van Nostrand, New York, 1967), chapter III.

18. H. Tatewaki and S. Huzinaga, J. Comp. Chem. 1, 205 (1980).

Figure captions.

Fig.1 Relative cross sections for reaction (1) as a function of vibrational quantum number v of $H_2^+(X^2\Sigma_g^+)$, obtained at the collision energies of 0.77 eV and 19.0 eV.

Fig.2 Relative cross sections for reaction (3) as a function of vibrational quantum number v of $O_2^+(X^2\Pi_g)$ and $O_2^+(a^4\Pi_u)$, obtained at the collision energies of 1.4 eV and 5.8 eV.

Fig.3 Relative cross sections for reaction (5) as a function of vibrational quantum number v of $NO^+(a^3\Sigma^+)$, obtained at the collision energy of 1.4 eV.

Fig.4 Ratios of the cross sections for the two spin-orbit states of $Ar^+(J=1/2, J=3/2)$ for reactions (2), (4), and (6) (left, middle, and right panels, respectively).
□ : experimental, —●— : calculated.

Fig.5 The $R(Ar-H_2)=\infty$ asymptote of the three low-lying potential energy surfaces of the $(Ar + H + H)^+$ system, with the spin-orbit

interaction of Ar^+ included.

Fig.6 Experimental cross sections for reaction (1) as compared with the calculated ones at the collision energies of 0.77 eV and 19.0 eV. ● : calculated, □ : experimental. The calculated and experimental values are nomalized at v=2.

Fig.7 The $R(Ar-O_2)=\infty$ asymptote of the five low-lying potential energy surfaces of the $(Ar + O + O)^+$ system, with the spin-orbit interaction of Ar^+ included.

Fig.8 Experimental cross sections for reaction (3) as compared with the calculated ones at the collision energy of 1.4 eV.

● : calculated, △ : experimental. The calculated and experimental values are normalized at v=5 of the $a^4\Pi_u$ state.

Fig.9 Experimental cross sections for reaction (5) as compared with the calculated ones at the collision energy of 1.4 eV.

● : calculated, □ : experimental. The calculated and experimental values are normalized at v=2.

Fig.10 The R(Ar-NO)=∞ asymptote of the four low-lying triplet potential energy surfaces of the $(Ar + N + O)^+$ system,

with the spin-orbit interaction of Ar^+ included.

Fig.11 The calculated potential energy curve of the ground triplet state ($^3A'$) as a function of the angle Θ the line of centers of the collision makes with the internuclear axis of NO. The bond length r(N-O) and the distance R between the center-of-mass of NO and Ar are fixed at 1.2 Å and 2.8 Å.

Fig.12 The calculated potential energy curve of the ground triplet state ($^3A'$) as a function of the distance R between the center-of-mass of NO and Ar. The bond length r(N-O) and the angle Θ the line of centers of the collision makes with the internuclear axis of NO are fixed at 1.2 Å and 90°, respectively.

Fig.13 The calculated potential energy curves of the triplet Π and Σ states in the collinear geometry as a function of the distance R between the center-of-mass of NO and Ar. The bond length r(N-O) is fixed at 1.2 Å. —●—: Π state, ---+---: Σ state.

Fig.14 The schematic potential energy curves for the two types of reaction mechanism of the $(BC + Ar)^+$ system. A: "Demkov type"

mechanism, B: "Landau-Zener type" mechanism.

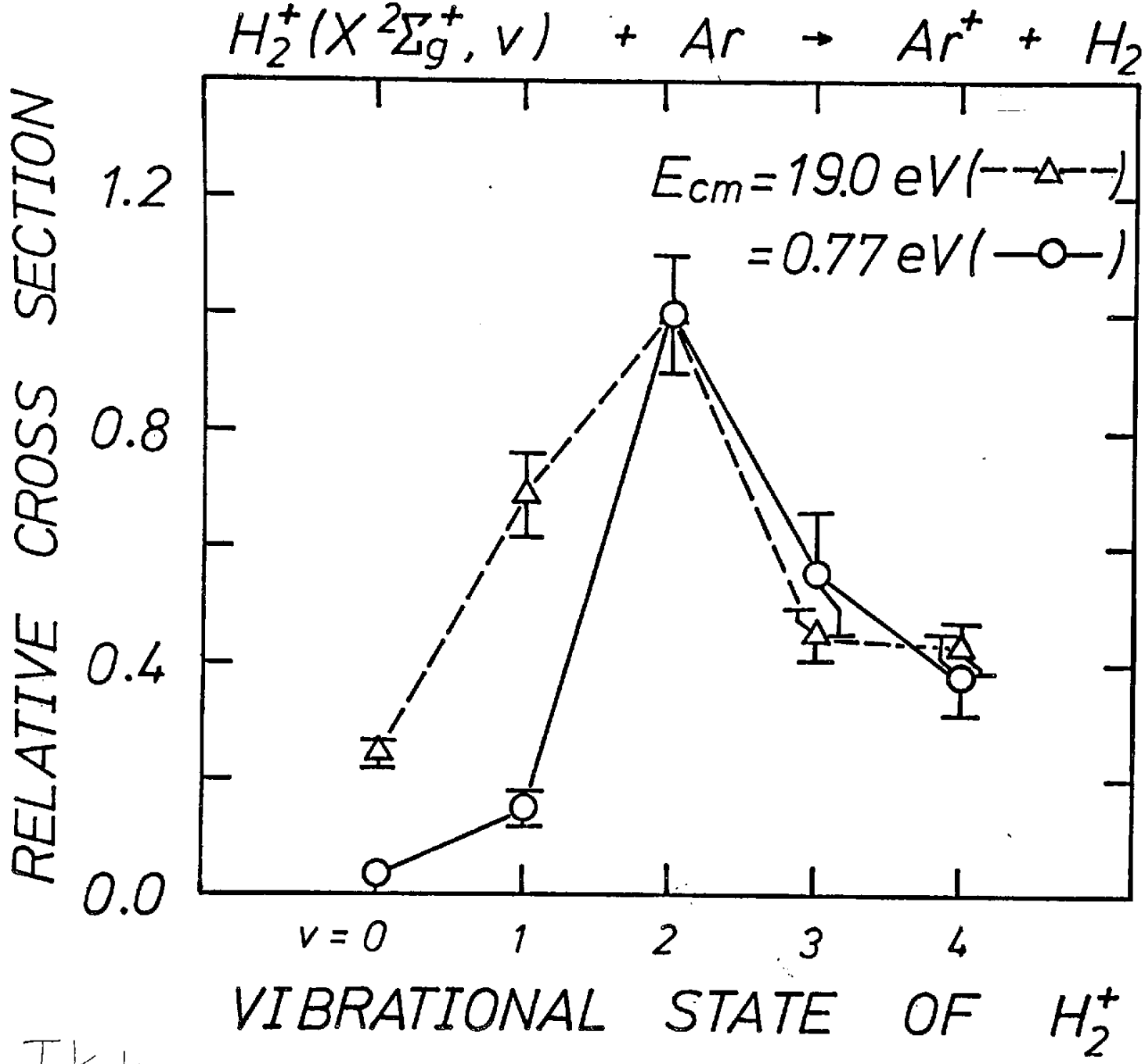
$H_2^+(X\,^2\Sigma_g^+, v) + Ar \rightarrow Ar^+ + H_2$
E_{cm} = 19.0 eV (--△--)
= 0.77 eV (—○—)
RELATIVE CROSS SECTION
1.2
0.8
0.4
0.0
v = 0
1
2
3
4
VIBRATIONAL STATE OF H_2^+

Fig. 1 T. Kato

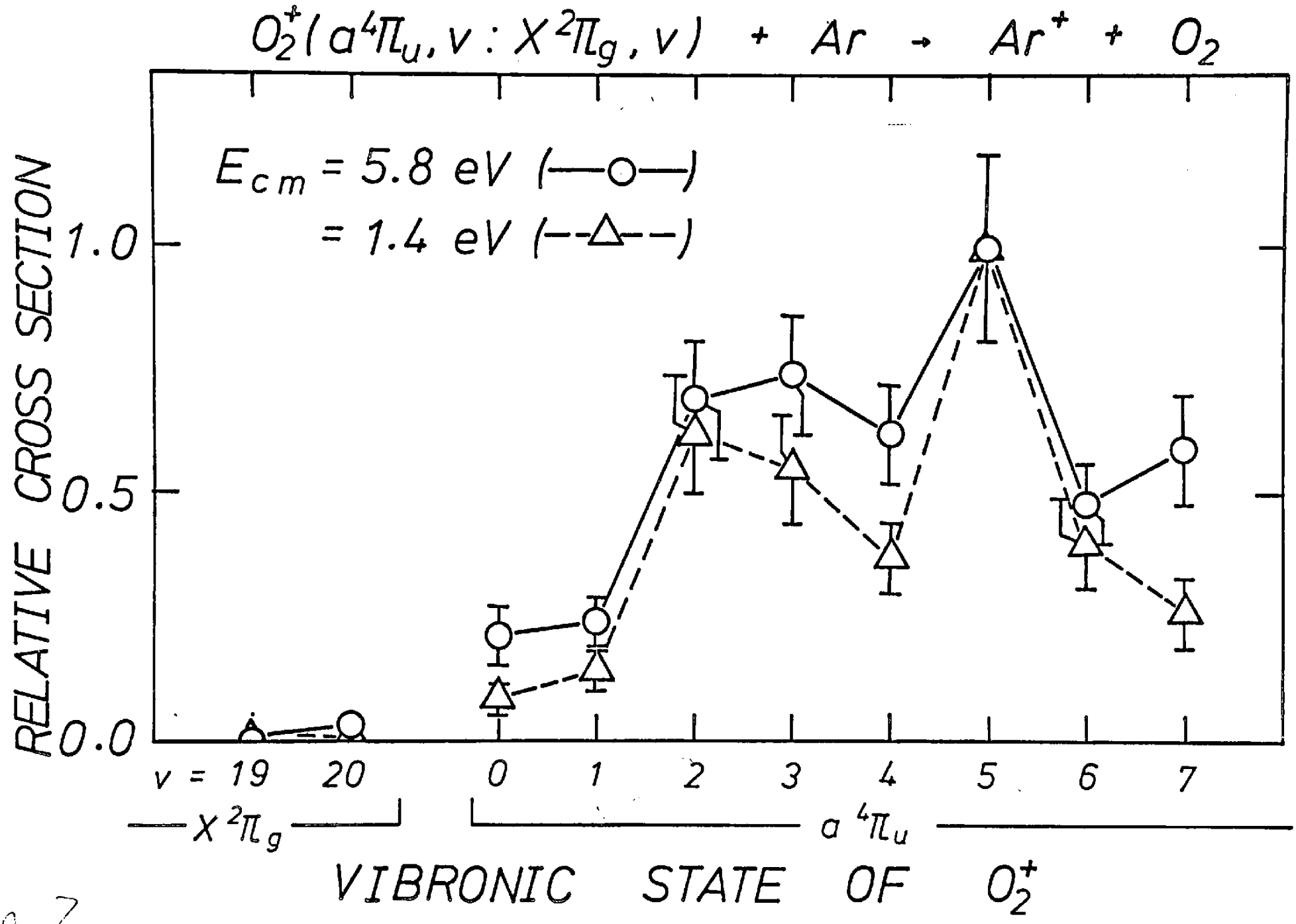
$O_2^+(a^4\Pi_u, v : X^2\Pi_g, v) + Ar \rightarrow Ar^+ + O_2$
E_{cm} = 5.8 eV (—○—)
= 1.4 eV (--△--)
RELATIVE CROSS SECTION
1.0
0.5
0.0
v = 19 20 0 1 2 3 4 5 6 7
$X^2\Pi_g$
$a^4\Pi_u$
VIBRONIC STATE OF O_2^+

Fig. 2 T. Kato

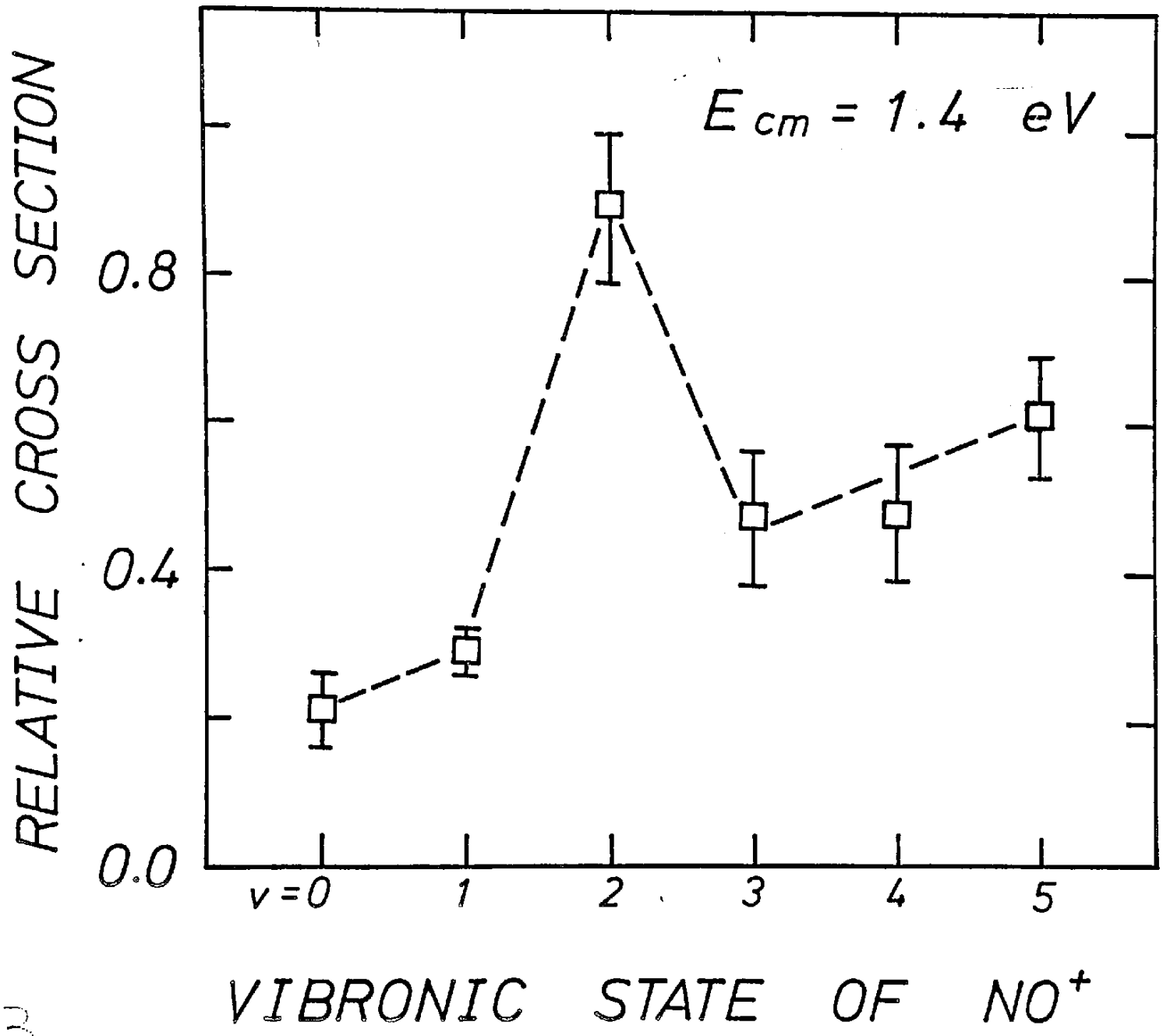
E cm = 1.4 eV
RELATIVE CROSS SECTION
0.0
0.4
0.8
v = 0
1
2
3
4
5
VIBRONIC STATE OF NO+

Fig. 3 T. Kato

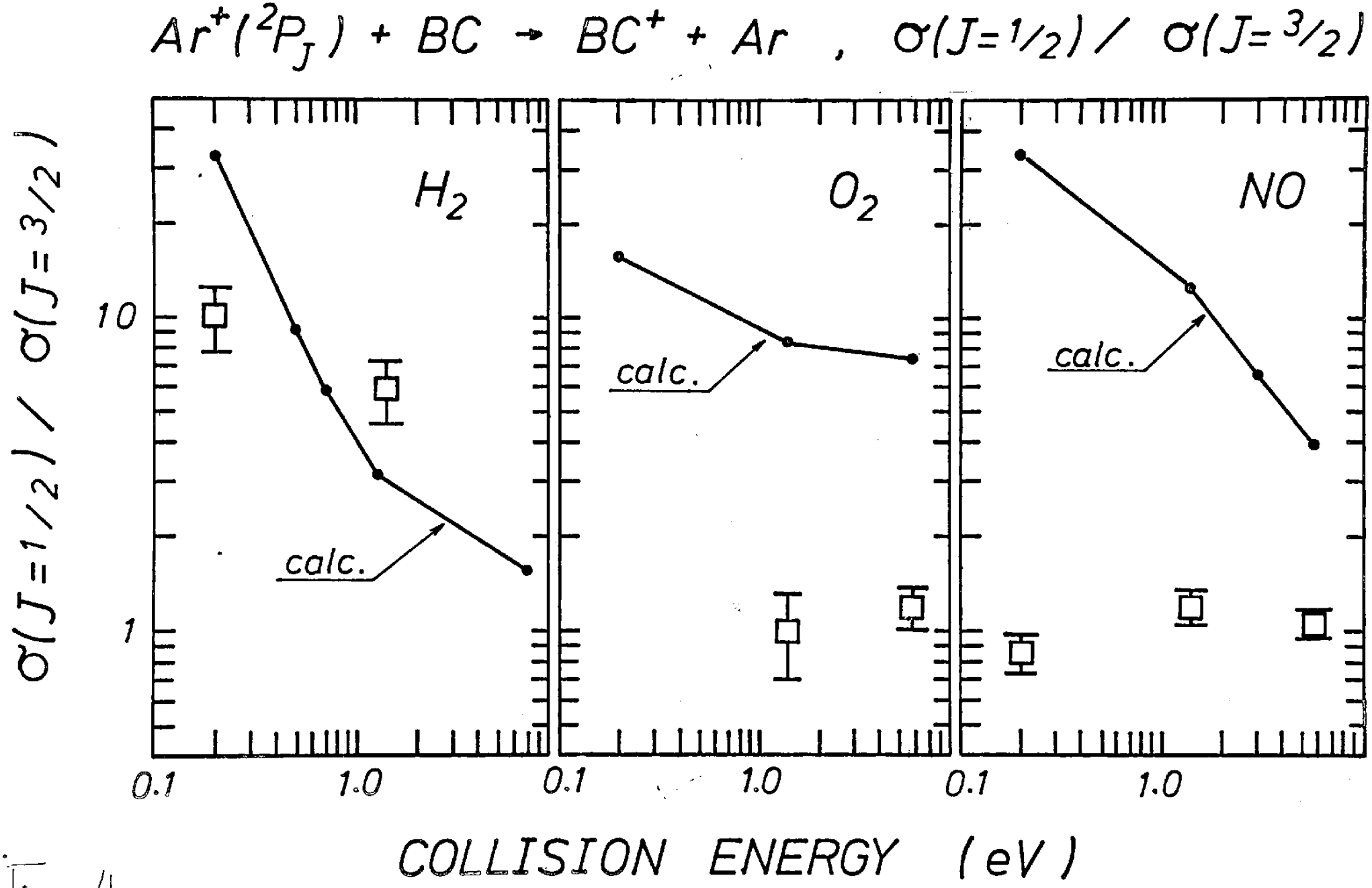
$Ar^+(^2P_J) + BC \rightarrow BC^+ + Ar$, $\sigma(J=1/2) / \sigma(J=3/2)$
$\sigma(J=1/2) / \sigma(J=3/2)$
10
1
H_2
O_2
NO
calc.
calc.
calc.
0.1
1.0
0.1
1.0
0.1
1.0
COLLISION ENERGY (eV)

Fig. 4

T. Kato

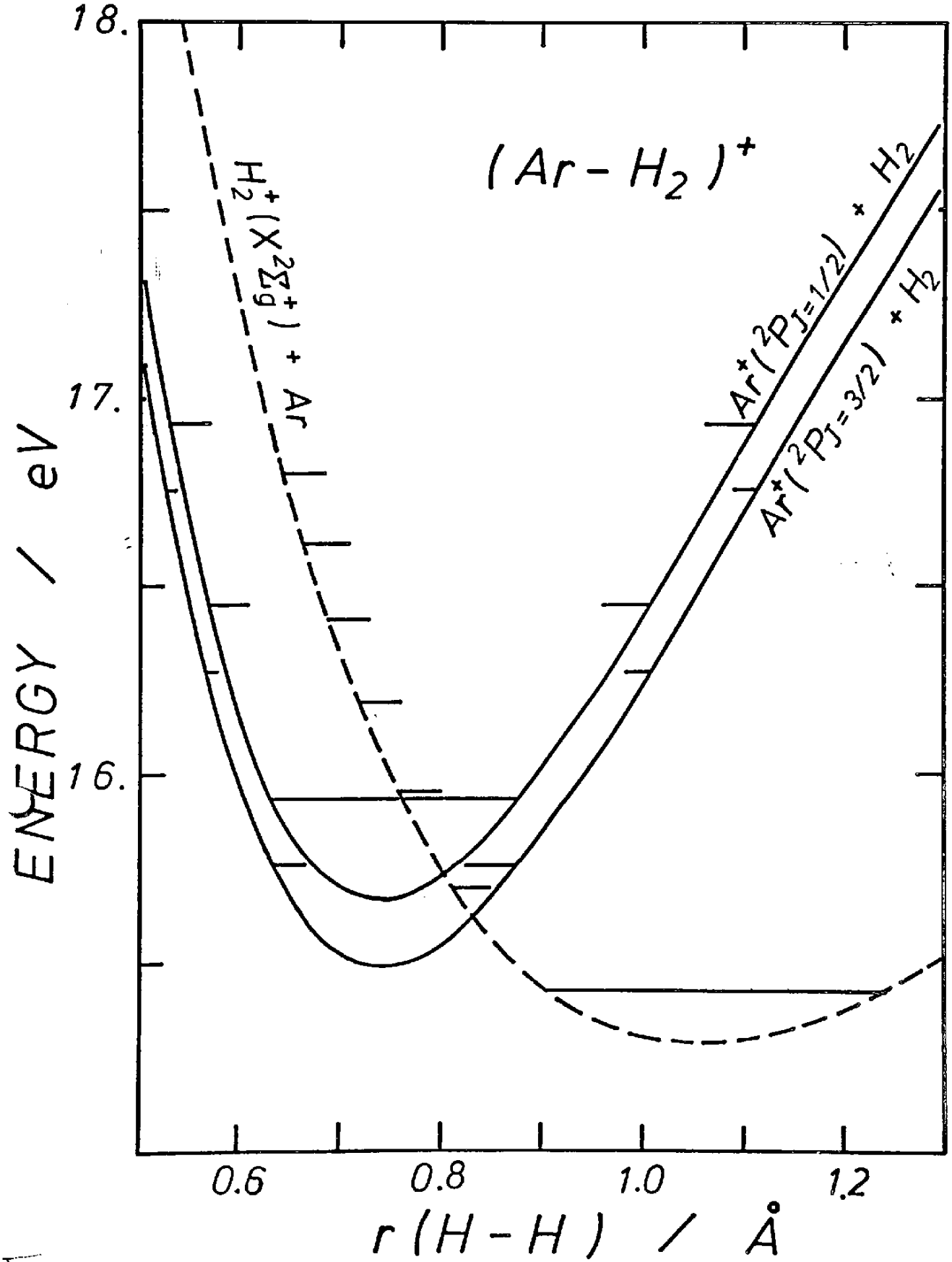
18.
17.
16.
ENERGY / eV
$(Ar-H_2)^+$
$H_2^+(X^2\Sigma_g^+) + Ar$
$Ar^+(^2P_{J=1/2}) + H_2$
$Ar^+(^2P_{J=3/2}) + H_2$
0.6
0.8
1.0
1.2
r (H - H) / Å

Fig.5 : T. Kato

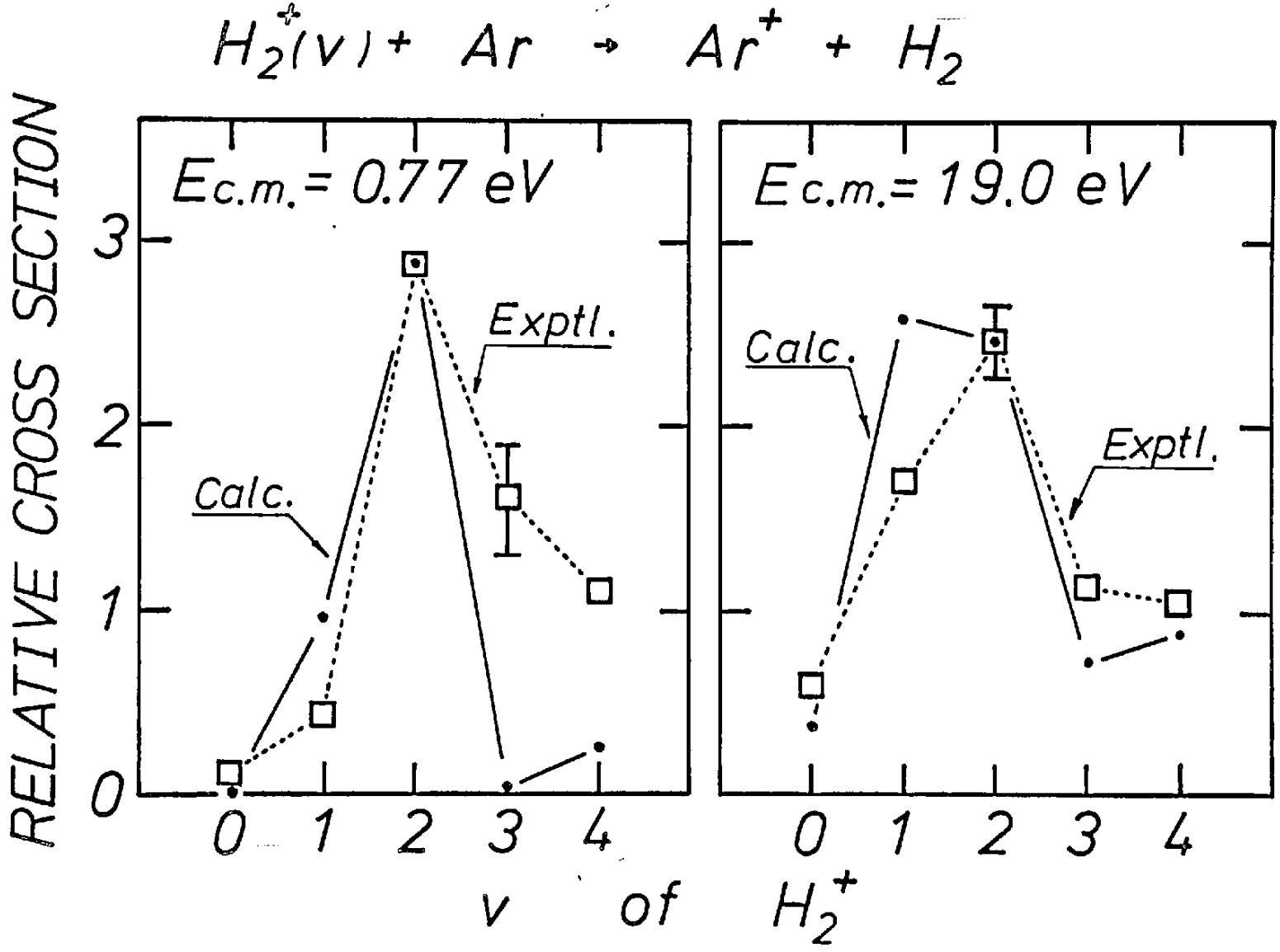
$H_2^+(v) + Ar \rightarrow Ar^+ + H_2$
RELATIVE CROSS SECTION
Ec.m.= 0.77 eV
Ec.m.= 19.0 eV
Exptl.
Calc.
Calc.
Exptl.
0
1
2
3
0 1 2 3 4
0 1 2 3 4
v of H_2^+

Fig.6

T Kato

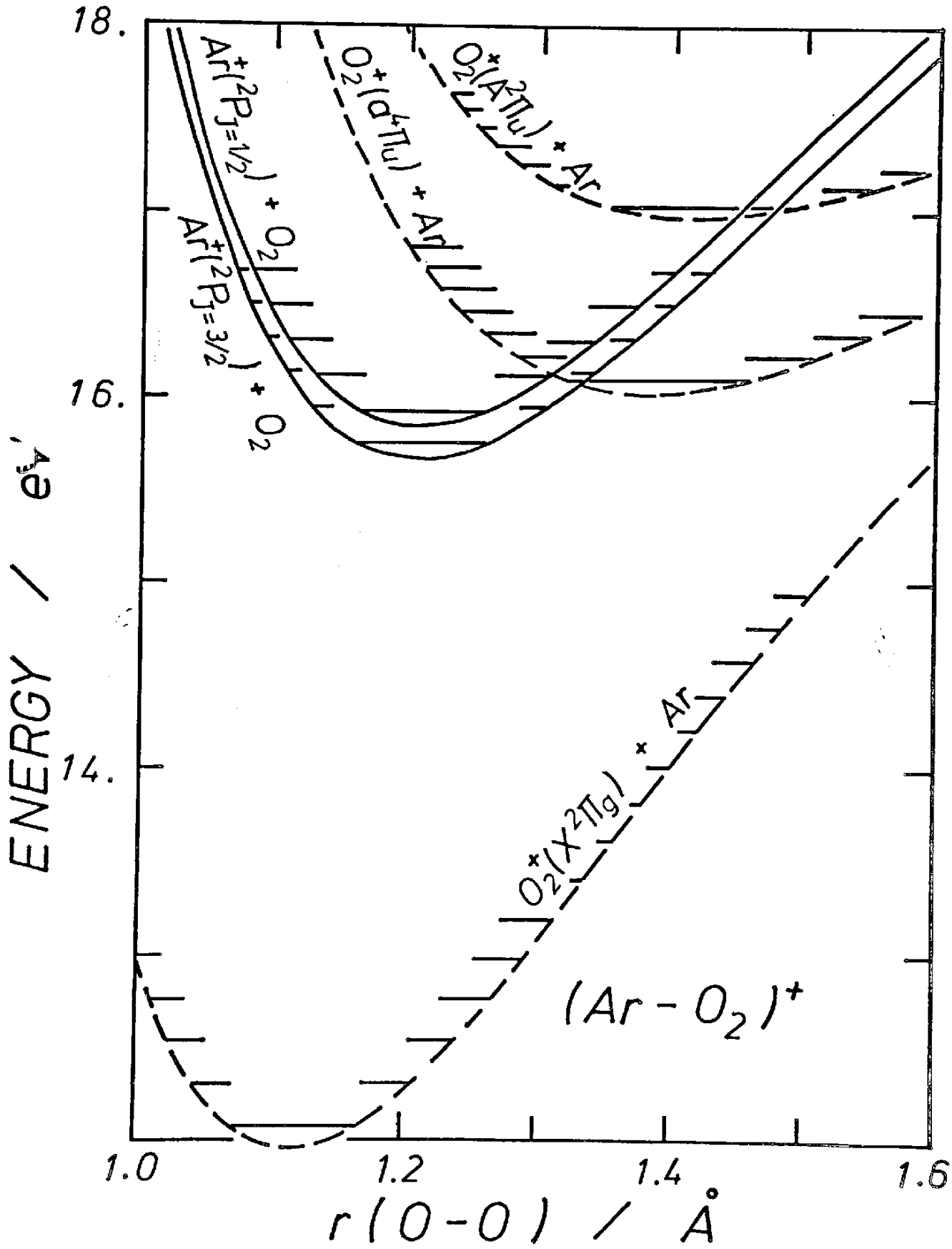
18.
16.
14.
ENERGY / eV
$Ar^+(^2P_{J=1/2}) + O_2$
$Ar^+(^2P_{J=3/2}) + O_2$
$O_2^+(a^4\Pi_u) + Ar$
$O_2^*(A^2\Pi_u) + Ar$
$O_2^*(X^2\Pi_g) + Ar$
$(Ar - O_2)^+$
1.0
1.2
1.4
1.6
r(O-O) / Å

Fig. 7 T. Kato

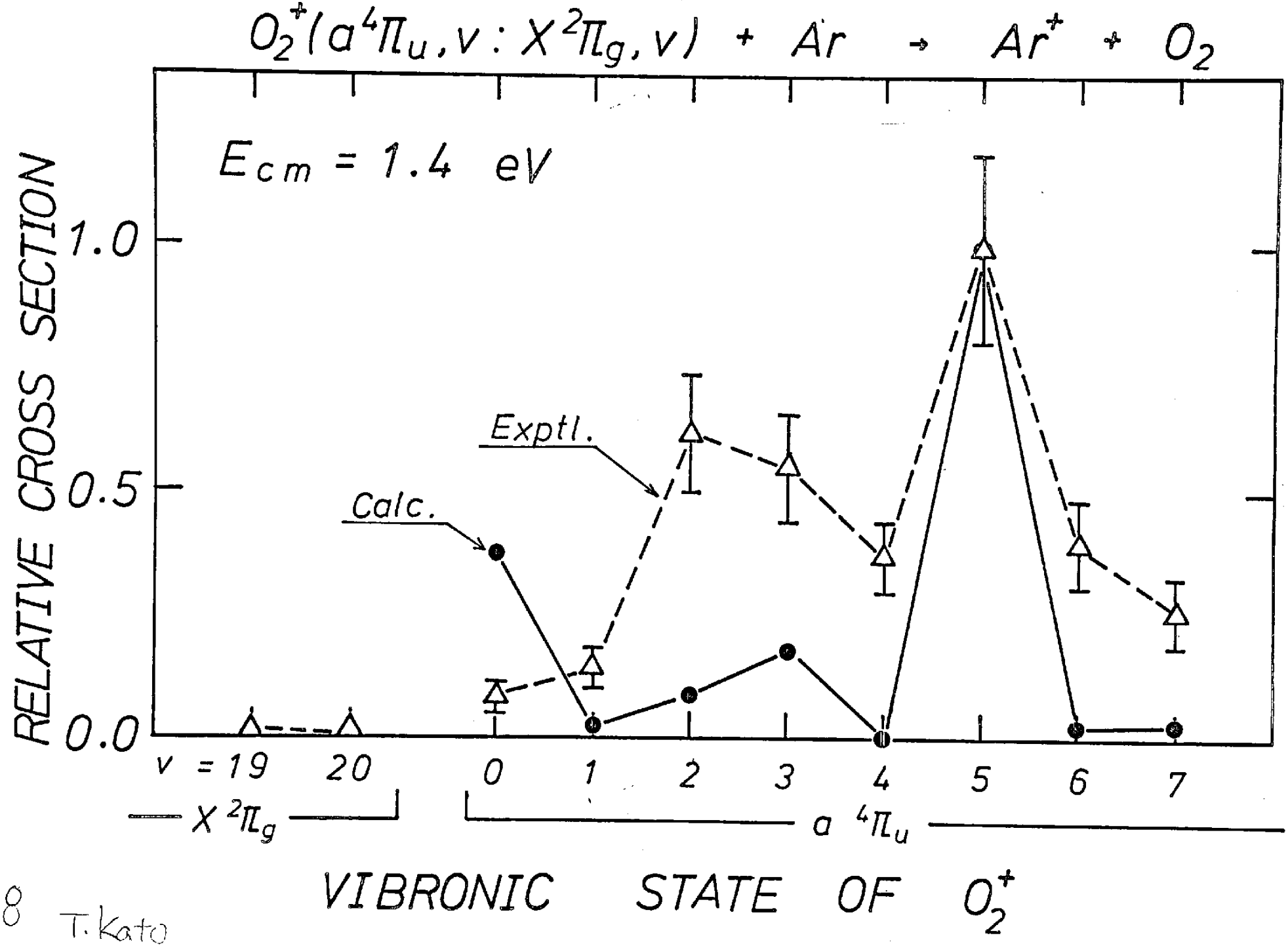
$O_2^+(a^4\Pi_u, v : X^2\Pi_g, v) + Ar \rightarrow Ar^+ + O_2$
$E_{cm} = 1.4$ eV
RELATIVE CROSS SECTION
1.0
0.5
0.0
Exptl.
Calc.
v = 19
20
0
1
2
3
4
5
6
7
$X^2\Pi_g$
$a^4\Pi_u$
VIBRONIC STATE OF O_2^+

Fig 8 T. Kato

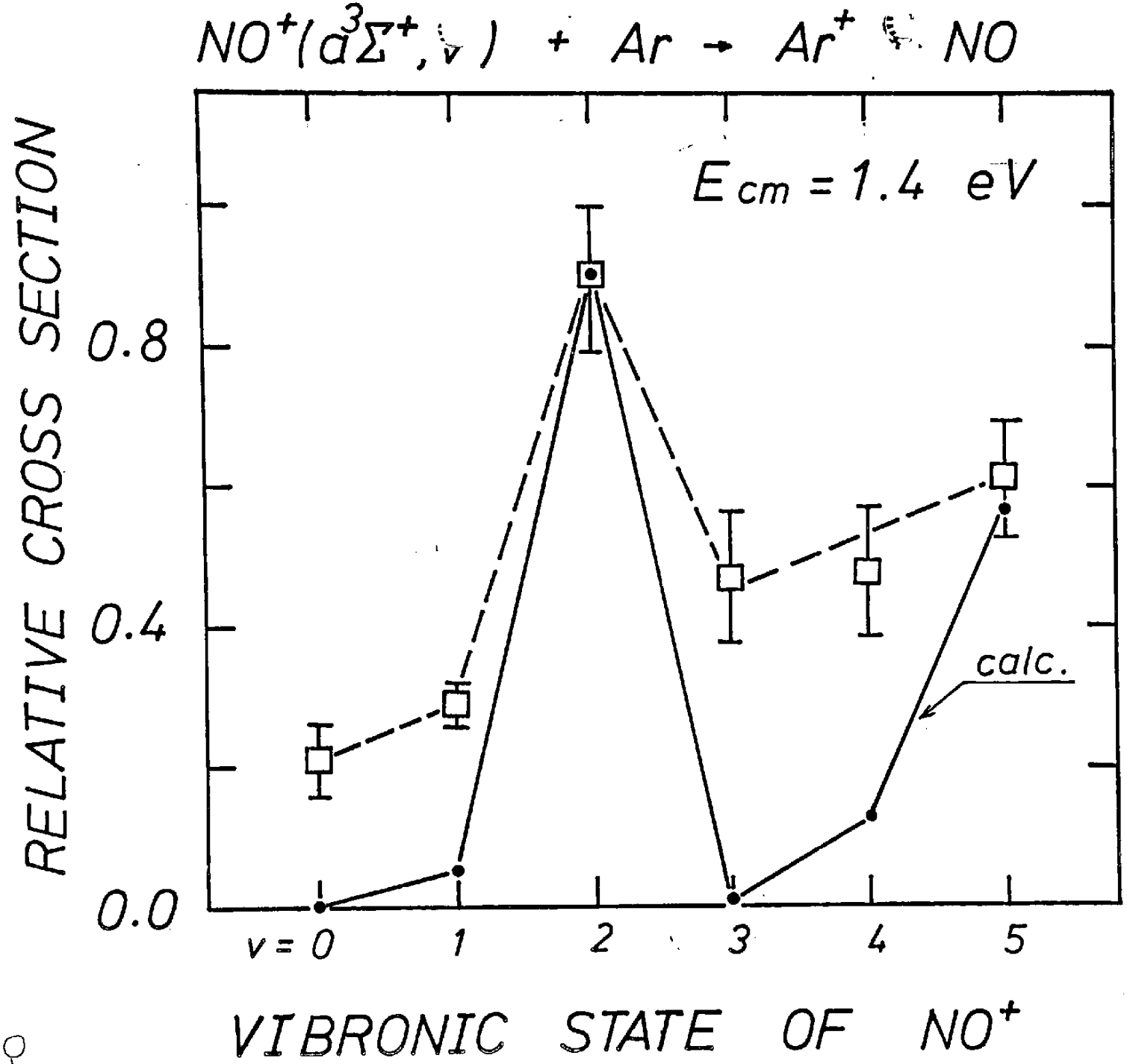
$NO^+(a^3\Sigma^+, v) + Ar \rightarrow Ar^+ + NO$
$E_{cm} = 1.4$ eV
RELATIVE CROSS SECTION
0.0
0.4
0.8
v = 0
1
2
3
4
5
calc.
VIBRONIC STATE OF NO^+

Fig 9 T. Kato

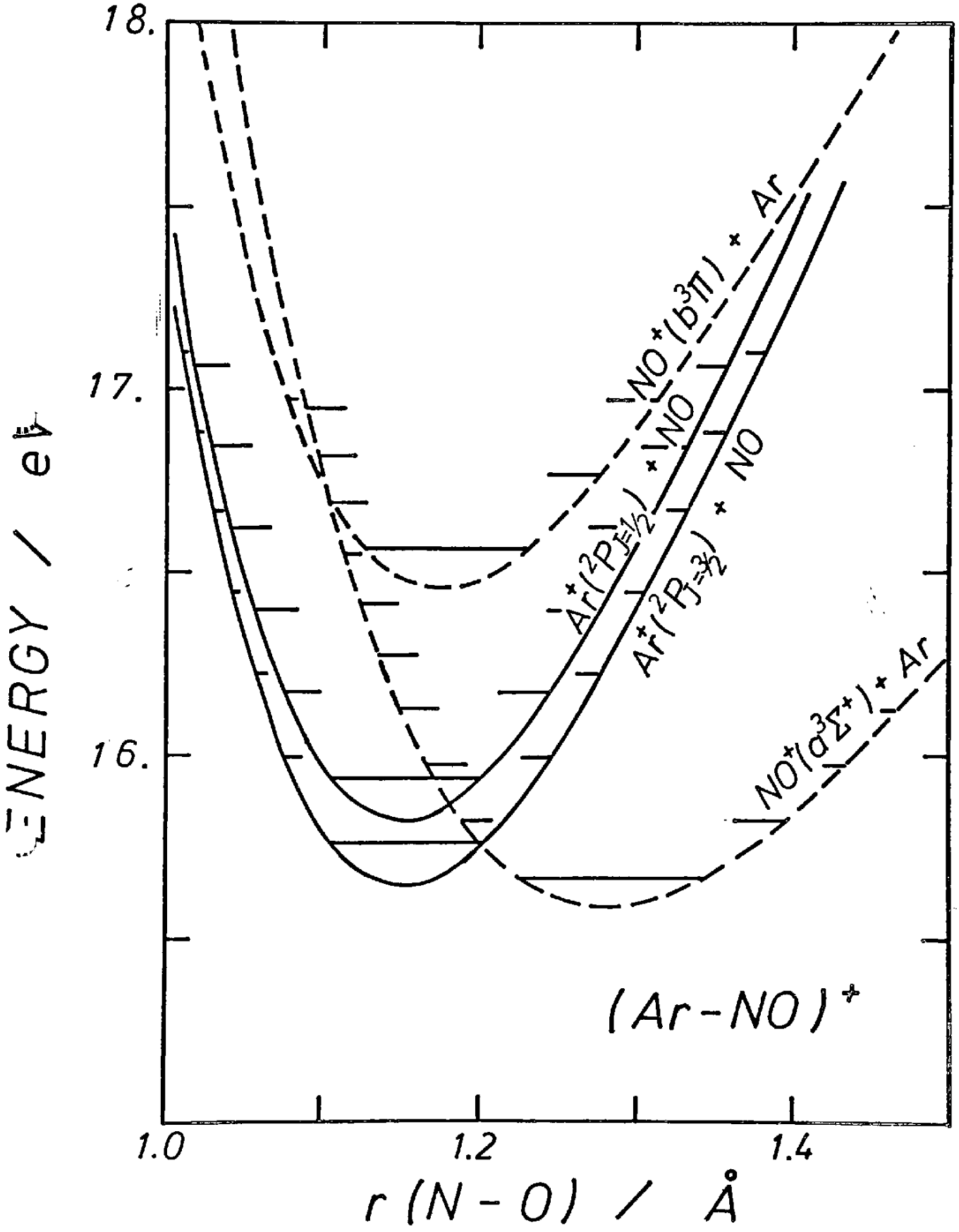
18.
17.
16.
ENERGY / eV
1.0
1.2
1.4
r (N - O) / Å
(Ar-NO)+
NO+(b3Π) + Ar
Ar+(2P1/2) + NO
Ar+(2P3/2) + NO
NO+(a3Σ+) + Ar

Fig. 10 T. Kato

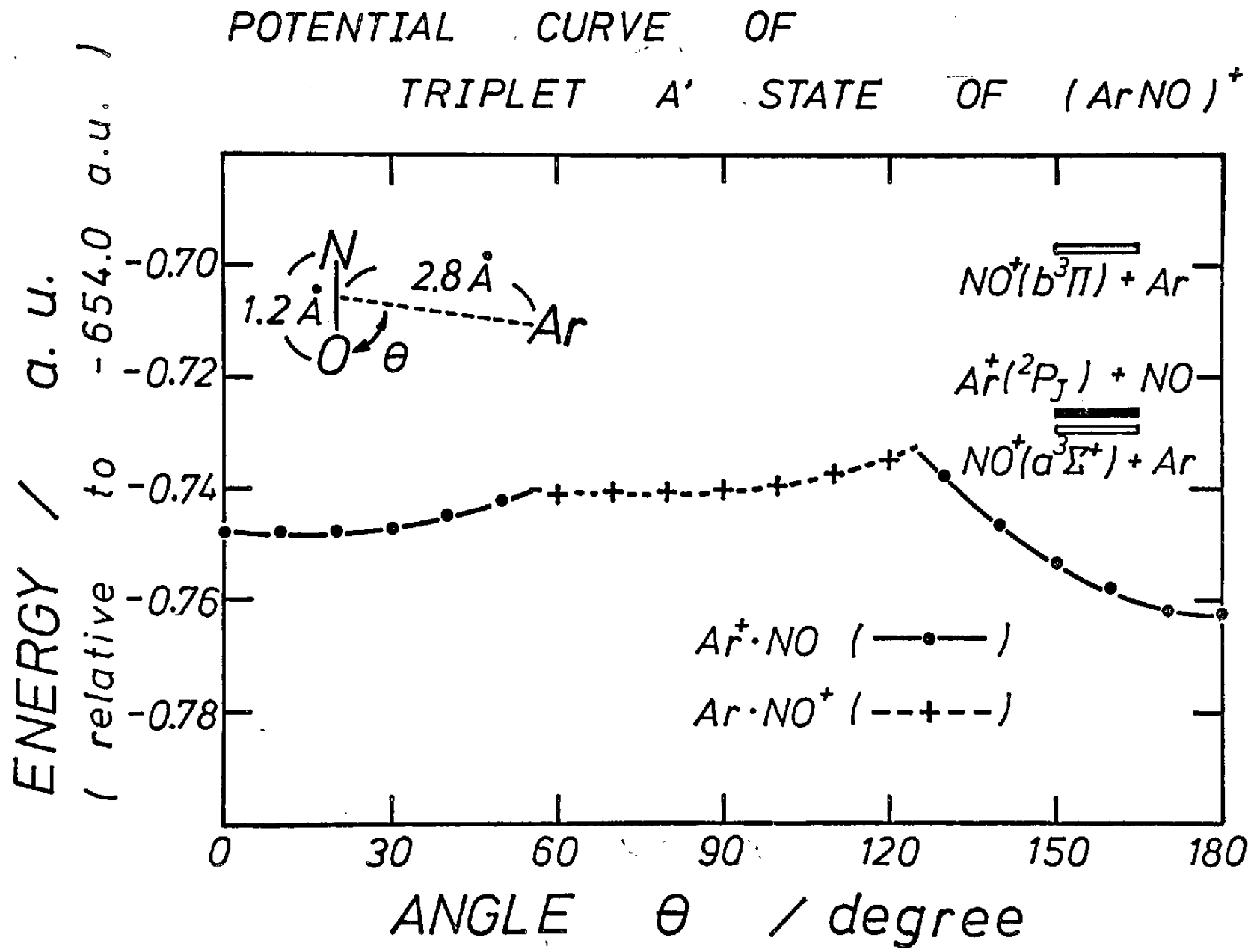
POTENTIAL CURVE OF
TRIPLET A' STATE OF (ArNO)+
ENERGY / a.u.
(relative to -654.0 a.u.)
-0.70
-0.72
-0.74
-0.76
-0.78
N
2.8 Å
1.2 Å
O
θ
Ar
NO+(b3Π) + Ar
Ar+(2PJ) + NO
NO+(a3Σ+) + Ar
Ar+·NO (—•—)
Ar·NO+ (--+--)
0
30
60
90
120
150
180
ANGLE θ / degree

Fig. 11 T. Kato

A POTENTIAL CURVE OF
TRIPLET STATE OF $(ArNO)^+$

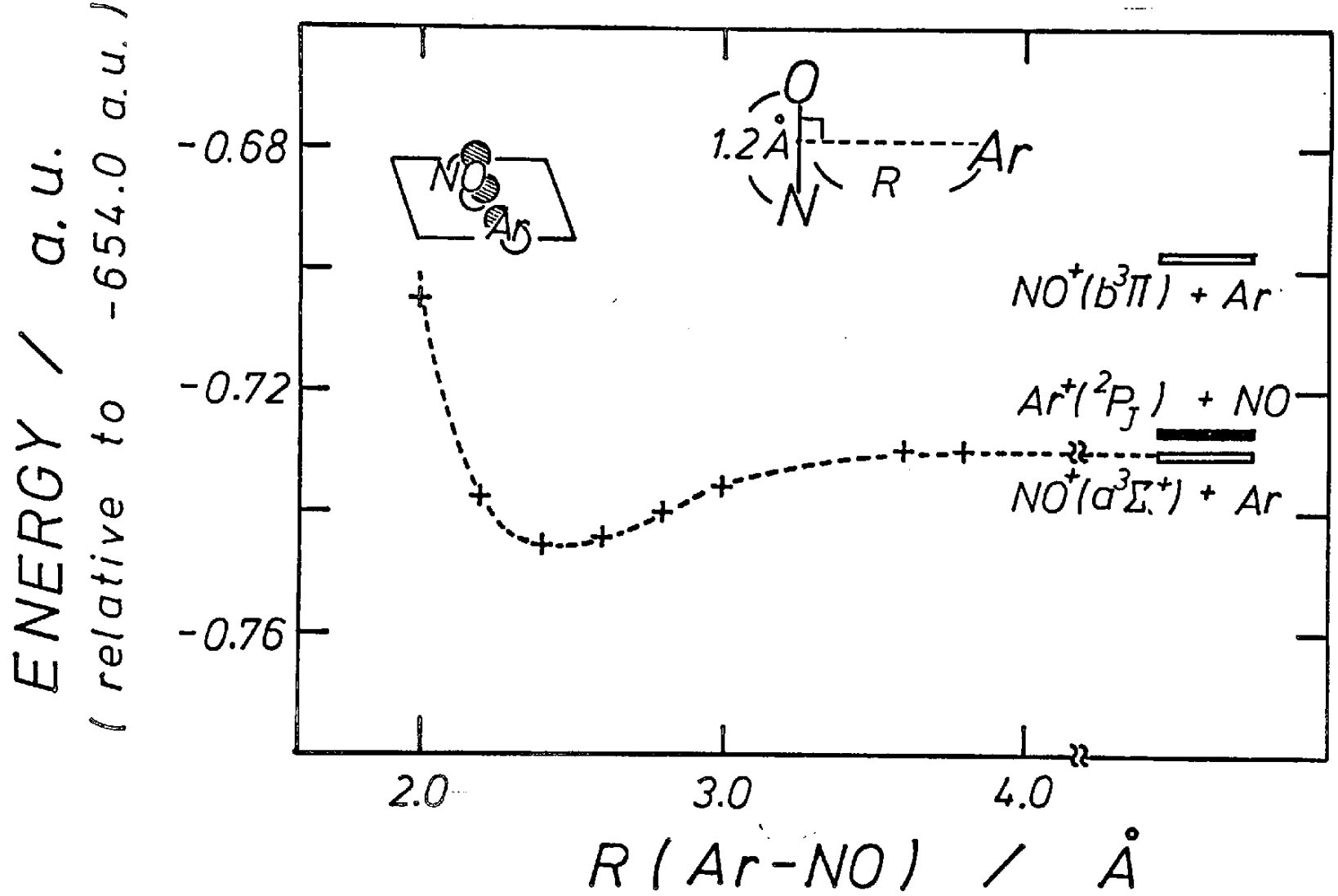

Fig. 12 T. Kato

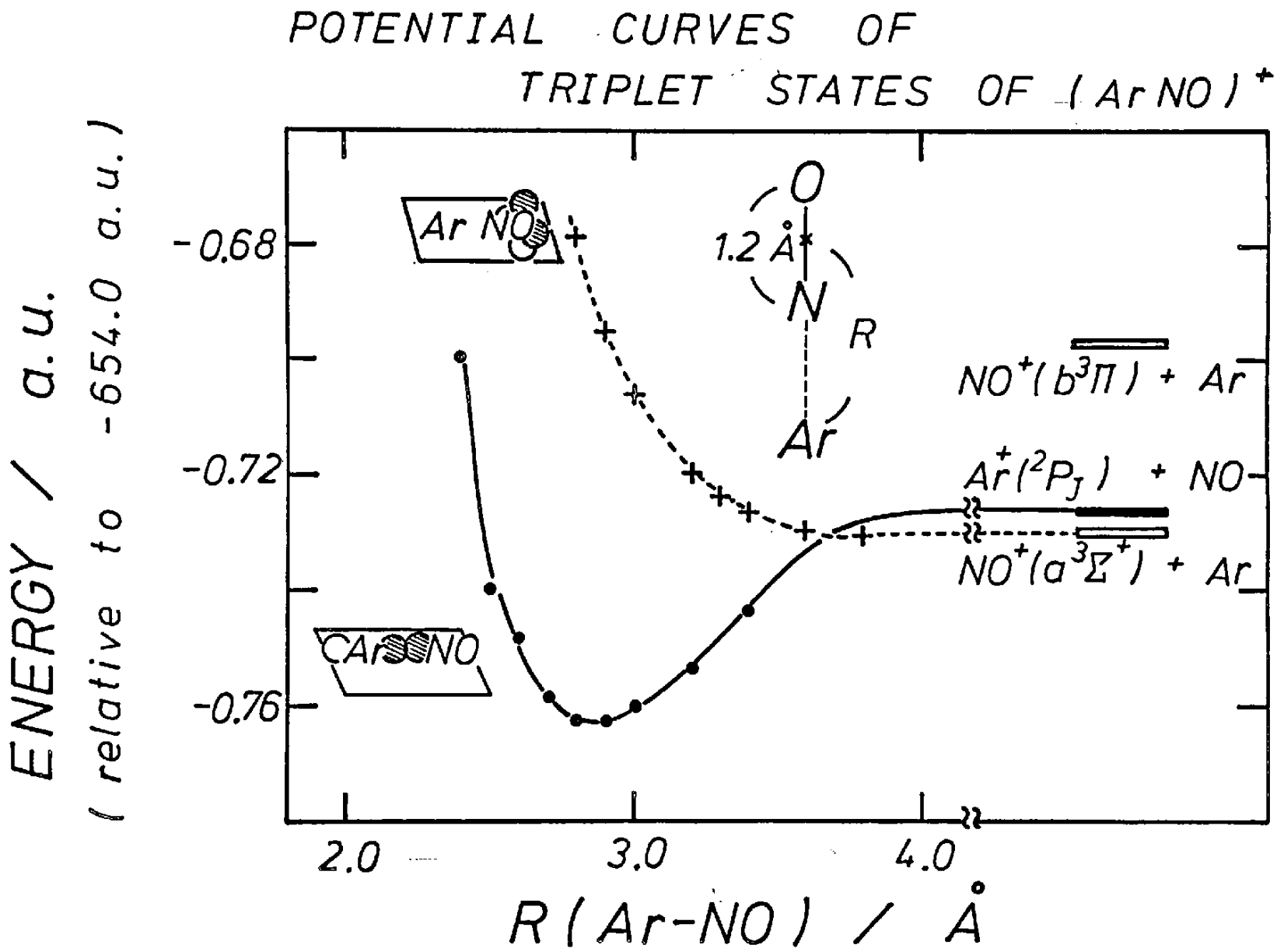
POTENTIAL CURVES OF
TRIPLET STATES OF (ArNO)+
ENERGY / a.u.
(relative to -654.0 a.u.)
-0.68
-0.72
-0.76
Ar NO
CArSCNO
O
1.2 Å
N
R
Ar
NO+(b3Π) + Ar
Ar+(2PJ) + NO
NO+(a3Σ+) + Ar
2.0
3.0
4.0
R(Ar-NO) / Å

Fig. 13 T. Kato

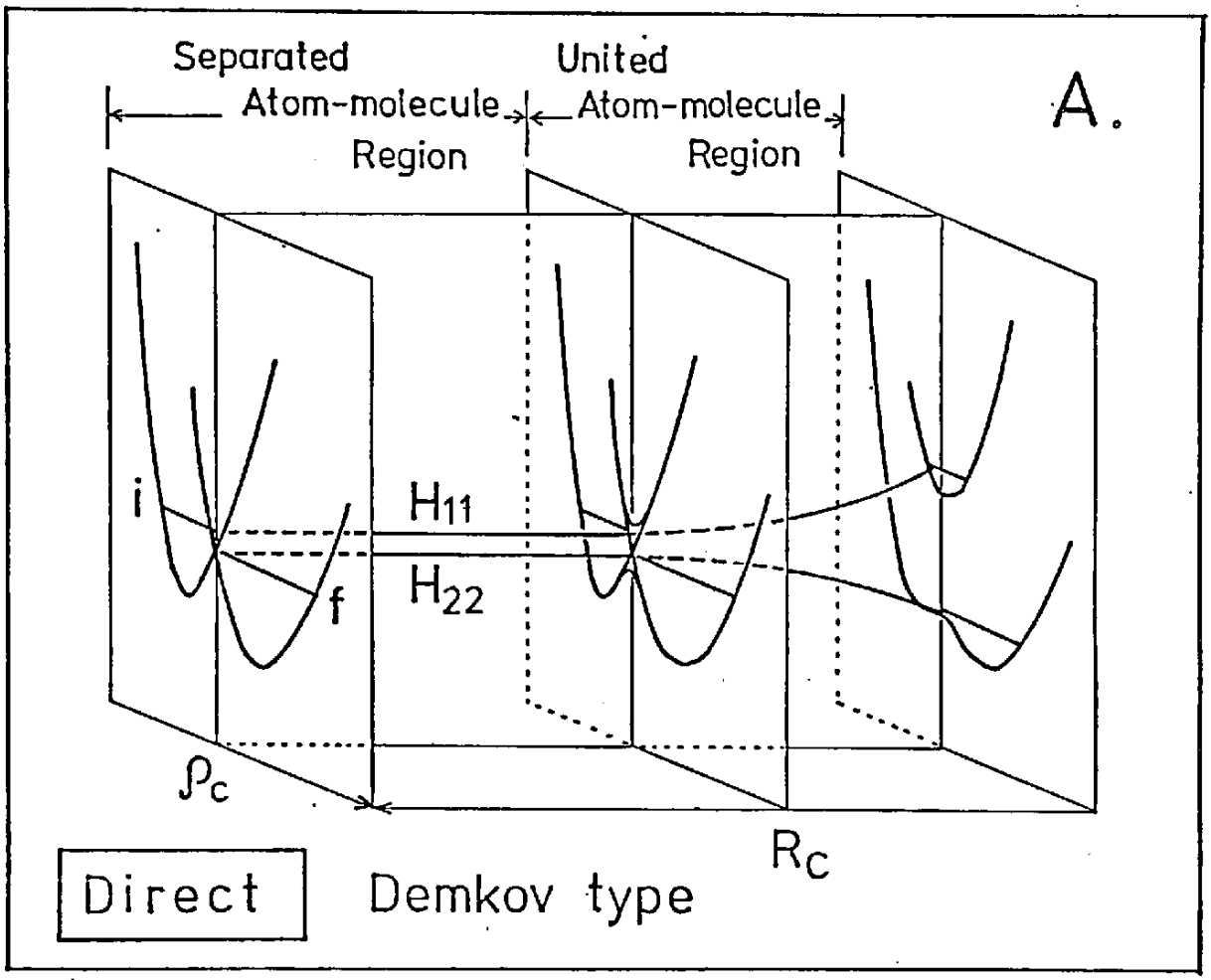
Separated
Atom-molecule
Region
United
Atom-molecule
Region
A.
i
f
H_{11}
H_{22}
ρ_c
R_c
Direct
Demkov type

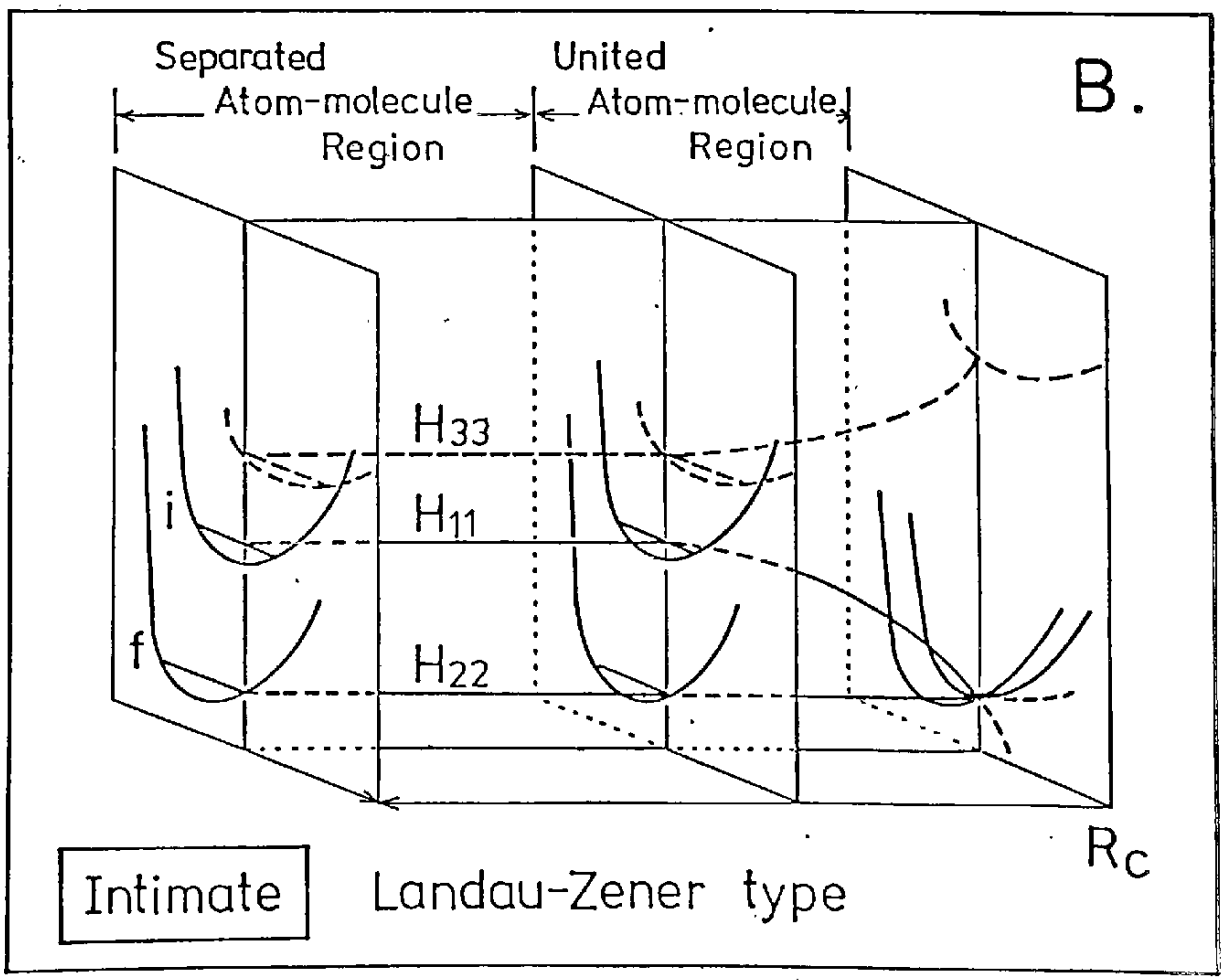
Separated
Atom-molecule
Region
United
Atom-molecule
Region
B.
H_{33}
H_{11}
H_{22}
i
f
R_c
Intimate
Landau-Zener type

Fig.14 T. Kato